Actomyosin Contractility is a Potent Suppressor of Mesoderm Induction by Human Pluripotent Stem Cells

Loic Fort[1,3], Wenjun Wang[2], and Ian Macara[1,3]

[1] Dept of Cell and Developmental Biology, Vanderbilt University School of Medicine Nashville TN 37240 USA

[2] Dept of Biomedical Engineering, Vanderbilt University Nashville TN 37240 USA

[3] Authors for correspondence

Abstract

The activation of WNT signaling in human pluripotent stem cells drives efficient conversion to lateral mesoderm, which can be further differentiated into cardiomyocytes. Stabilization of the WNT effector β-catenin promotes expression of mesoderm-specifying genes such as Brachyury (Bra/T, encoded by *TBXT*) and Eomesodermin and drives an epithelial-mesenchymal transition (EMT) that occurs at 49-52 hrs post WNT activation. Interestingly, WNT activation also triggers an early contraction of stem cell colonies, with increased myosin light chain (MLC) phosphorylation, resulting to cellular morphological changes. Small molecule inhibitors and genetic approaches were applied to determine if contractility is related to mesoderm differentiation. Contrary to expectation, suppressing contractility accelerated differentiation; Bra/T induction was enhanced, and EMT initiated as early as 24 hrs post WNT activation. Conversely, expression of constitutively active Rho kinase or myosin light chain kinase, to increase contractility, efficiently blocked any induction of mesoderm, including EMT. Mechanistically, reduced contractility promoted active β-catenin levels in the cytoplasm and nucleus. We propose that the early contraction of human pluripotent stem cell colonies in response to WNT activation initially delays mesoderm induction by restraining accumulation of active β-catenin, suggesting a role for contractility as a temporal gate.

Introduction

Mechanical forces play major roles at many stages of animal development: Starting as early as embryo compaction at the 4-cell stage[1], forces are crucial through gastrulation and later during tissue morphogenesis. Internal forces are largely generated by acto-myosin contractility, and in epithelia are transmitted across cell boundaries by intercellular junctions, enabling collective organization. Tension is generated by these junctions and by adhesion to the extracellular matrix (ECM). Early embryogenesis is marked by waves of cell fate specification to create the three major lineages, followed by further differentiation, and these events are likely coordinated with changes in physical forces created by the cells, to which they then respond. Mechanistically, however, the connections between cell fate and mechanical force remain unclear.

Human embryonic stem cell (hESC) and induced pluripotent stem cell (hiPSC) colonies can be induced to select the mesoderm lineage and eventually to differentiate into functional cardiomyocytes. Pluripotent stem cells are strongly epithelial and lineage specification relies on an epithelial-to-mesenchymal transition (EMT) that is reminiscent of some aspects of gastrulation. When treated with the morphogen BMP4, hESCs can self-organize into 2D "gastruloids" [2], and if plated on compliant hydrogel surfaces they will form "gastrulation-like" nodes that express Brachyury, a mesoderm marker. Micropatterning and traction stress mapping demonstrated that regions of high tension promote Brachyury expression, through release of β-catenin from the cell junctions and consequent activation of WNT signaling, which is known to be required for mesoderm induction [3].

Mesoderm can also be generated from human pluripotent stem cells by direct WNT pathway activation using the small molecule GSK3β inhibitor Chiron 99021 (hereafter CHIR), which protects β-catenin from degradation. Whether mechanical forces play any role in this pathway to mesoderm induction is unknown. We observed that hiPSCs induced by CHIR to differentiate into mesoderm show colony contraction, increased phospho-MLC (myosin light chain) and increased optical retardance, which is a non-invasive measure of actomyosin contractility. From this correlation between contractility and mesoderm induction, plus prior work on BMP4-driven mesoderm in hESCs, we expected that inhibiting actomyosin activity would block induction. Surprisingly, however, we obtained the opposite result: suppressing MLC phosphorylation using small molecule inhibitors or genetic tools substantially promoted mesoderm induction, while

58 further increasing actomyosin contractility was sufficient to block differentiation and EMT
59 completely. Mechanistically, we found that promoting cell relaxation led to an increase in active
60 β-catenin in the cytoplasm and nucleus.
61
62 **Results**
63 WNT-mediated mesoderm specification increases actomyosin contractility
64 To explore how cells sense, integrate and respond to physical cues, we first investigated
65 whether differentiating cells experience differential forces along their conversion from hiPSC to
66 mesoderm. hiPSCs were treated with CHIR to stabilize β-catenin and thereby activate the WNT
67 pathway, triggering pluripotency exit and commitment to primitive streak and mesoderm
68 lineages. We noticed that hiPSC colonies showed rapid retraction of their edgea following CHIR
69 addition **(Supp. Fig 1A)**, consistent with observations from other groups [4]. Having previously
70 reported an essential and permissive role for apoptosis during mesoderm specification [5], we
71 tested whether colony retraction was related to the wave of cell death that occurs following
72 CHIR addition. However, co-treatment with a pan-Caspase inhibitor (Q-VD-OPH) did not affect
73 retraction of colony edges **(Supp. Fig 1A)**, ruling out an effect of cell density and cell death.
74 Commitment to the mesoderm lineage also resulted in thicker epithelial layers,
75 containing taller cells **(Supp. Fig 1B-D)**, suggesting profound morphological changes that are
76 highly dependent on the cellular contractile state. Consistent with the role of nuclei as
77 mechanosensor [6,7], differentiating cells exhibit significantly smaller nuclear area after 48h of
78 CHIR treatment **(Supp. Fig 1E-F)**. To address the variation of cell density, we correlated each of
79 our nuclear area measurements with the actual cell number **(Supp. Fig 1G)**. As expected,
80 nuclear area negatively correlates with cell density before differentiation. However, we did not
81 find any correlation following CHIR treatment, together suggesting that the smaller nuclear size
82 at 48h of differentiation is unlikely to be related to cell density. While these observations were
83 indirect, they point towards a differential contractile status of early in mesoderm commitment,
84 switching from low contractile undifferentiated cells to high contractility. To directly test for
85 higher contractility, differentiating cells were stained for phospho-T18/S19 Myosin Light Chain 2
86 (ppMLC), a key regulator of contractility. Immunofluorescences reveal a gradual increase of
87 ppMLC2 intensity over time, with the formation of supracellular fibers extending across several
88 cells **(Supp. Fig 1H-I)**. Finally, we took advantage of the birefringence property of actin fibers to

89 measure light retardance using quantitative polarization microscopy. Birefringence of a material
90 changes proportionally to the applied strain, providing an orthogonal way to probe for
91 contractile status during mesoderm commitment. Confirming our previous data, retardance
92 values increased during hiPSC-to-mesoderm conversion **(Supp. Fig 1J)**. Specificity of the
93 retardance value as a readout for contractility was tested by incubating undifferentiated hiPSCs
94 with a ROCK inhibitor (Y-27632) to suppress MLC phosphorylation. Together, these data suggest
95 that hiPSC differentiating along the cardiac mesoderm trajectory experience increasing
96 contractile forces mediated by MLC2 activity.
97
98 <u>Inhibition of actomyosin contractility promotes hiPSc and hESC conversion to the mesoderm</u>
99 <u>lineage</u>
100 We hypothesized that increased contractility might be required for pluripotent cell to
101 acquire their mesoderm identity. To test this hypothesis, hiPSCs were differentiated in the
102 presence of ROCK inhibitor, Y-27632. We first confirmed that MLC2 phosphorylation was
103 reduced by ROCK inhibition **(Supp. Fig 2A-B)**. Contrary to expectations, blocking contractility
104 strongly promoted Brachyury expression, a mesoderm marker (encoded by the *TBXT* gene, also
105 known as *T* gene) **(Fig 1A-B)**. Expression of other key mesoderm (*MESP1* and *TBX6*) and EMT
106 (*SNAI1* and *SNAI2*) genes was also upregulated following Y-27632 treatment **(Fig 1C-F)**. To rule
107 out an effect for ROCK inhibition on global transcription, we examined expression levels of
108 genes unrelated to mesodermal fate and did not detect any response to decreased contractility,
109 suggesting a specific role of actomyosin contractility in cell fate specification **(Supp. Fig 2C)**.
110 Normal hiPSCs synchronously undergo EMT at 49-52hrs post-CHIR addition. Brachyury
111 expression is initially restricted to the colony edges at 24hrs, before broader expression across
112 the colony at later timepoints (**Fig. 1G-H**). However, Y-27632 treatment resulted in markedly
113 accelerated EMT, as shown by loss of the epithelial marker ZO-1 from tight junctions (**Fig. 1G, I**)
114 and increased expression of the mesenchymal marker Slug **(Supp. Fig 2D**), plus more
115 widespread Brachyury expression **(Fig. 1G-H)**. To validate these data, we used the more specific
116 ROCK inhibitor, H-1152, which led to similar decreases in ppMLC2 **(Supp. Fig 2E-F)** and
117 recapitulated the early EMT and higher induction of mesoderm markers **(Supp. Fig 2G-M)**.
118 Importantly, these effects of ROCK inhibition were conserved in hESCs expressing a knock-in T-
119 mNeonGreen fusion [3] **(Fig. 1J-K)** and in wild-type H9 hESCs treated with CHIR. Importantly,

120 there was no effect of reduced contractility on exit from the pluripotency state **(Fig 1L and**
121 **Supp. Fig 2N, P)**.
122 Because apoptosis-mediated ATP release is crucial to enable mesoderm fate
123 specification [5], we probed for PARP cleavage as an apoptosis marker but did not detect any
124 difference following addition of Y-27632 or H-1152 **(Supp. Fig 2L and 2N-O)**. MLC2
125 phosphorylation was previously shown to be spatially regulated by ROCK and Myosin Light
126 Chain Kinase (MLCK) in polarized and non polarized cells [8,9]. Therefore, we tested the
127 involvement of MLCK by treating cells with ML-7, a potent MLCK inhibitor [10]. ML-7 led to
128 efficient reduction in ppMLC2 **(Fig. 1N-O)** and strongly enhanced Brachyury expression at 48h
129 **(Fig. 1P-Q),** without affecting cell death. Together these data unexpectedly shows that
130 pharmacological blocking of MLC2-mediated force generation enhances mesoderm
131 commitment quantitatively and accelerates the EMT required for conversion to the cardiac
132 mesoderm.
133
134 <u>Genetic suppression of actomyosin contractility promotes stem cell conversion to the</u>
135 <u>mesoderm lineage</u>
136 To rule out off target effects of the small molecule inhibitors, we designed a genetic
137 approach to suppress contractility in human cells. Dephosphorylation of ppMLC is mediated by
138 Myosin Light Chain Phosphatase, an heterotrimer composed of a catalytic subunit PP1cβ, a
139 Myosin phosphatase-targeting regulatory subunit (MYPT1) and a protein of unknown function
140 M20 [11,12] (**Fig 2A-B**). Based on previous work describing an optogenetic construct to control
141 actomyosin contractility [13], we created a truncated MYPT1, fused with a nuclear export
142 sequence and a mNG reporter (**Fig 2B**), that is expected to act as a constitutively active mutant
143 and promote MLC2 dephosphorylation. To validate the activity of this new tool, we cloned this
144 construct (referred to as $MYPT1^{CA}$-NES-mNG) under a doxycycline-inducible promoter and
145 established a stable hiPSC line. Global reduction of ppMLC2 was observed by immunoblot and
146 immunofluorescence after doxycycline addition (**Fig 2C-E**). Strikingly, activating $MYPT1^{CA}$
147 recapitulated the effects of pharmaceutical inhibition of contractility: differentiating $MYPT1^{CA}$
148 cells displayed enhanced Brachyury expression (**Fig 2F-J**) and earlier induction of the EMT genes
149 Snail and Slug (**Fig 2F**) following Doxycycline induction, compared to controls. Apoptosis

150 induction was not affected in this system (**Fig 2H**). We conclude that reducing MLC2-driven
151 contractility using both pharmaceutic and genetic strategies, accelerates mesoderm identity.
152
153 Contractility is a potent inhibitor of mesoderm identity
154 Next, we sought to test if constitutively increased contractility impacts hiPSC-to-mesoderm
155 conversion. We stably expressed constitutively active ROCK2 or MLCK ($ROCK2^{CA}$ and $MLCK^{CA}$)
156 under a doxycycline inducible promoter with ubiquitous expression of a mVenus reporter. Green
157 transduced cells were mixed with unlabeled WT hiPSCs, pre-treated or not with doxycycline to
158 turn on $ROCK2^{CA}$ or $MLCK^{CA}$ before starting the differentiation protocol for 72h (**Fig 3A**). We first
159 confirmed that mVenus-positive cells treated with doxycycline showed signs of higher
160 contractility. In the co-culture set up with $ROCK2^{CA}$/WT or $MLCK^{CA}$/WT cells treated with
161 Doxycycline, mVenus-positive clusters showed strong cortical F-actin and higher ppMLC2
162 staining organized as fibers compared to WT mVenus-negative cells which show more diffused
163 staining (**Supp. Fig 3A, C**). These data support the idea that mVenus-positive cells experience
164 higher contractility, allowing us to test whether cell fate was affected. $ROCK2^{CA}$/WT co-cultures
165 were treated with water (+ Veh) or Doxycycline (+Dox) and stained for mesoderm (Bra/T) (**Fig.**
166 **3B**), primitive streak (EOMES) (**Fig 3D**) and EMT markers (Slug and ZO-1) **(Fig 3F**). mVenus-
167 positive and negative area were drawn based on the mVenus coverage across each cluster
168 (**Supp. Fig 3B-D**) and percentages of cells expressing each marker were reported. Following
169 doxycycline induction, mVenus-positive clusters showed a dramatic decrease in mesoderm,
170 primitive streak and mesenchymal markers compared to mVenus-negative cells or Vehicle-
171 treated cells (**Fig. 3C-E-G**). Because we previously showed that MLCK inhibition affects
172 mesoderm commitment the same way as ROCK inhibition (**Fig. 1P-Q**), we sought to address the
173 effect of MLCK-driven contractility on cell identity. Importantly, $MLCK^{CA}$-positive clusters failed
174 to commit to the primitive streak and mesoderm lineage and to trigger the EMT program
175 required for mesoderm identity (**Supp. Fig 3E-G**). These data support the hypothesis the
176 surprising conclusion that constant and pre-mature activation of ROCK/MLCK-mediated
177 contractility prevents mesoderm conversion and EMT and is sufficient to counteract the effect
178 of CHIR.
179
180 Reduced cell contractility promotes nuclear accumulation of stable β-Catenin

181 Mechanistically, we first hypothesized that Hippo signaling, one of the main mechanosensitive
182 pathways in epithelial tissues, drives mesoderm identity enhancement upon cell relaxation. YAP,
183 a downstream effector of the Hippo pathway, has been previously associated with cell fate
184 patterning in 2D gastruloids [14] Activation of the Hippo pathway leads to phosphorylation of YAP
185 at Ser127, restricting its localization to the cytosol and promoting degradation. In contrast, non-
186 phosphorylated YAP translocates to the nucleus and forms a complex with co-transcriptional
187 activator TEAD1-4, together regulating gene expression. Surprisingly, however, phosphorylated
188 YAP is not affected during differentiation or by cell relaxation (**Supp. Fig 4 A-B**). We next directly
189 probed for *CTGF* and *CYR61* expression, two well-described YAP target genes. Gene expression
190 strongly decreased during differentiation but was not affected by cellular contractile status
191 (**Supp. Fig 4C**). Together, these data rule out a significant role for the Hippo pathway in the
192 acceleration of mesodermal differentiation following cell relaxation.
193 Next, we investigated the positive feedback loop reported during BMP4-driven
194 mesoderm commitment, which relies on mechanical tension-dependent secretion of canonical
195 WNT ligands [3]. We treated our MYPT1^{CA}-NES-mNG cells with doxycycline to trigger cell
196 relaxation and probed for canonical and non-canonical WNT ligands. As a positive control,
197 expression of the mesoderm marker *TBX6* was increased in low contractile cells compared to
198 Vehicle-treated control cells. Interestingly, canonical WNT ligand expression (*WNT3A* and
199 *WNT8A*) was strongly upregulated by suppression of contractility, while non-canonical *WNT4*
200 expression was unaffected by CHIR treatment nor by the reduction of contractility (**Supp. Fig**
201 **4E**). To test whether increased WNT3A/8A expression was responsible for increased mesoderm
202 commitment in low-contractility cells, we blocked WNT ligand processing and secretion using
203 IWP-2 (Porcupine inhibitor). Addition of IWP-2 did not rescue mesoderm gene expression in Y-
204 27632-treated cells, suggesting that this pathway is unlikely to drive mesoderm specification
205 enhancement (**Supp. Fig 4F**).
206 We then turned our attention to β-catenin, which exists in epithelial cells both as a
207 cytosolic molecule and bound to E-Cadherin at adherens junctions and plays key
208 mechanosensitive functions during development and tissue homeostasis [3,15]. Whether each
209 pool shares common regulatory mechanisms is still debated [16]. In the absence of WNT signaling,
210 cytosolic β-catenin is associated with a destruction complex, where it is phosphorylated at
211 Ser45 by CK1, which primes the protein for subsequent phosphorylation by GSK3β, driving its

212 ubiquitination and degradation. WNT activation disrupts the destruction complex, permitting
213 the accumulation of stable, non-phosphorylated β-catenin. Therefore, active non-phospho β-
214 catenin (hereafter active β-catenin) signaling can be assessed from the level of non-
215 phosphorylated Ser45. We evaluated active β-catenin shuttling to the nucleus by isolating
216 cytosolic and nuclear fractions from MYPT1^{CA} cells (**Fig 4A**). Purity of each fraction was assessed
217 from enrichment of a nuclear and cytosolic marker, Lamin A/C and GAPDH respectively (**Supp.**
218 **Fig 4D**). Strikingly, active β-catenin was strongly upregulated in both the cytosolic and the
219 nuclear fractions in low contractile differentiating cells (24h + Dox) (**Fig. 4B, C**). Immunostaining
220 confirmed the enrichment of active β-catenin in the nucleus 24h post differentiation (**Fig. 4D-F**).
221 We validated this observation by imaging a mEGFP-β-Catenin knock-in line treated with CHIR in
222 normal or low contractility (Y-27632) states. First, we noticed cytosolic accumulation of mEGFP-
223 β-catenin within 5h of CHIR treatment, regardless of the presence of Y-27632. However,
224 consistent with the immunostaining data, mEGFP-β-catenin later became enriched in the nuclei
225 of cells under low contractile stress (**Supp. Fig 4G-H**). Collectively, these findings suggest that a
226 cell relaxation-dependent nuclear accumulation of β-catenin potentiates the WNT signaling-
227 dependent mesoderm program. However, this model can only hold true if the concentration of
228 CHIR used in our system (7.5 µM) does not saturate the WNT signaling response. To test this
229 premise, we doubled the concentration of CHIR and probed for expression of WNT target genes
230 as a read-out for WNT signaling (**Fig. 4G**). *LEF1* and *AXIN2* expression responded in a dose-
231 dependent manner to CHIR. Interestingly, however, at any given CHIR concentration, inhibition
232 of cell contractility by addition of Y-27632 further enhanced WNT-target gene responses.
233 Together, these results demonstrate that increased active β-Catenin translocation to the nucleus
234 following cell relaxation amplifies WNT response and enhances mesoderm commitment, in a
235 synergistic way with CHIR.
236
237 **Discussion**
238 Synchronization of developmental processes is key to development. Germ cell lineage
239 commitment relies on tight spatio-temporal control of genetic programs, which is concomitant
240 to profound morphological changes during gastrulation. Here, we aimed to investigate how
241 differentiating cells sense and integrate physical cues. Our data reveal an unexpected and
242 paradoxical role for acto-myosin contractility as a potent inhibitor of the mesoderm lineage. We

243 report that low contractility promotes nuclear localization of β-catenin, which correlates with
244 higher mesoderm marker expression. β-catenin exists as two pools, one bound to the adherens
245 junctions through E-Cadherin and one cystosolic pool, part of the WNT pathway. The regulation
246 and exchange of β-catenin molecules between these 2 pools remains poorly understood. E-
247 Cadherin binding to β-catenin prevents its nuclear translocation and co-activator transcriptional
248 activity [17] SRC-mediated phosphorylation of β-catenin at residue Y654 reduces by 6-fold the
249 binding interaction [18] so one possibility might be that SRC activity is dependent on contractility
250 in pluripotent stem cells. Alternatively, Gayrard et al [19] reported a mechanism by which release
251 of cell-cell tension is required for β-catenin release through SRC-dependent phosphorylation of
252 FAK. Therefore, release of tension leads to β-catenin accumulation in the cystosolic
253 compartment and its translocation into the nucleus as observed by cell fractionation and
254 confocal imaging (Fig. 4B, D and Supp. Fig 4G).

255 In several in vivo and in vitro models, including ours, initiation of mesoderm commitment
256 correlates with tissue deformation and cell contraction [3,20–23]. In *Drosophilia,* contraction of the
257 posterior end of the embryo is mediated by supercellular active myosin II cables reminiscent
258 with our observation in 2D [24]. Higher contractility also leads to deformation of nuclear
259 morphology, as reported by others [21,25]. Therefore, how can we reconciliate this response with
260 the fact that reducing contractility promotes mesoderm identity? We propose a model in which
261 increasing contractility following the first 24h of differentiation dampens CHIR response to
262 temporally synchronize mesoderm identity. Indeed, in the developing embryo, specification of
263 lineages required deep morphological changes and cell compaction occur, mostly mediated by
264 actomyosin contractility [26–28]. It is widely accepted that high density cells, similar to ingressing
265 cells during gastrulation, have low contractility compared to cells at low density, both in vitro
266 and in vivo [29]. Our work suggest that this mechanical gate prevents mesoderm identity until
267 mechanical tension is released. Inducing low contractility prior to CHIR treatment, disrupts this
268 mechanical gate, resulting to accelerated mesoderm identity and EMT.

269 Our data demonstrate that contractile forces are strongly antagonist for mesoderm induction
270 They confirm and expand on a previous study using Y-27632 to enhance mesendodermal
271 differentiation [30], while ruling out potential off target effect of the drug. Our study also suggests
272 that cell fate can be modulated by actomyosin contractility. In *Xenopus,* decreased ROCK-

273 dependent actomyosin contractility promotes ectoderm-to-mesoderm transition, with
274 ectodermal cells adopting mesoderm-like properties [31], together emphasizing the plasticity of
275 cell fate during development. While we have not tested for alternative cell fate following CHIR
276 addition, our differentiation protocol was adapted from Lian et al [32,33] and was not reported to
277 lead to ectodermal identity. Additionally, we note that differentiating cells lose their
278 pluripotency marks, regardless of their contractile status, suggesting that the rate of
279 pluripotency exit is not affected (Supp. Fig 2N, P).
280 We further report that low contractile cells show premature EMT and induction of mesoderm
281 specification, and link it to higher nuclear β-catenin signaling. These findings balance previous
282 reports suggesting that mechanical tension promotes Brachyury expression in Bilateria [34] and in
283 gastrulation-like models, through mechanosensitive regulation of β-catenin at high cell adhesion
284 tension [3]. Muncie et al proposed a dual function for mechanical tension: First, BMP4-driven
285 Brachyury expression relies on mechanical stretch of cell junction that triggers a β-catenin-
286 mechanosensitive response by exposing the conserved Y654 residue. Phosphorylation by SRC-
287 family kinase destabilizes junctional β-catenin and initiates its nuclear translocation. A positive
288 feedback loop reinforces mesoderm commitment through increased canonical WNT ligand
289 secretion. These discrepancies may be explained by differences in the differentiation protocol
290 (BMP4 versus CHIR) and possibly by the substrate/micropattern used [35], providing differential
291 biochemical and mechanical inputs. Indeed, our protocol directly activates WNT pathway by
292 inhibition of the destruction complex, which is in contrast with BMP4 activation. Moreover,
293 while we noticed increased canonical WNT ligand expression following cell relaxation, we ruled
294 out a feed-forward loop by blocking WNT ligand secretion (Supp. Fig 4D-E).
295 Alternative mechanisms might also complement this pathway. For instance, a previous study
296 shows that hiPSC epithelial cohesiveness is a crucial barrier for BMP4-signaling activation, by
297 blocking BMP4 diffusion to the basolaterally-localized BMP receptors and restricting Brachyury
298 expression to the colony edge [36]. However, in our system, the use of the small molecule GSK3β
299 inhibitor CHIR as a differentiating cue rules out a similar initial mechanism. While WNT target
300 genes have now been extremely well characterized in multiple systems, it remains unclear how,
301 β-catenin affects temporally its effectors. The dynamics nature of β-catenin, and the plasticity of
302 WNT activation in undifferentiated cells [37], may explain the different outcomes resulting from
303 specific differentiation protocols.

Recent reports highlight the extreme sensitivity of hiPSC to cell density. For example, the key mechanical transducer ETV4 was linked to cell crowding and fate determination, with an ON/OFF response dependent on cell density [38]. Similarly, radial patterning of 2D gastruloid was strongly affected by a 1.5 fold change in cell density, while WNT dynamics was affected by only a 1.15 fold increase of cell density [39]. In our system, we showed that while nuclear area tends to correlate with cell density in basal condition, this correlation was lost during differentiation. Additionally, cell density is highly linked with Hippo pathway activity and we showed that Hippo pathway is not differentially regulated during mesoderm induction, confirming previous data from our lab at a later timepoint [5]. Unlike other studies on mammary cell lines [40] we did not notice any effect of ROCK inhibition on YAP phosphorylation state. One explanation might be that PSCs are strongly epithelial and, as previously reported, are insensitive to Hippo activation-dependent cell-cell interaction[41].

Limitations of the study

In this study, we aimed to understand if and how mechanical tension is important for mesoderm lineage specification. To this end, we used a simple 2D system, allowing us to control most parameters while only perturbing actomyosin contractility. However, this 2D system is limited by its physiological implication. Translation of these data into 2.5D and 3D models of gastrulation (2D and 3D gastruloid respectively), and alternatively into early mouse development will allow the generalization these findings. Moreover, while we consistently observed higher β-catenin in the nucleus upon cell relaxation, further work will be required to address whether it reflects an increase of import or a decrease of export from the nucleus.

Finally, it remains to address whether increased nuclear β-catenin results to an increase binding to its target gene promoters, such as Brachyury promoter, which contains two TCF/LEF-1/β-catenin binding sites within the first 500pb [42,43]. Alternatively, further work on chromatin rearrangement will be required to better understand whether enhancer/repressor get spatially modulated by mechanical tension.

Acknowledgements

We thank Cynthia Reinhart-King for giving us access to the QPOL facility. We thank the Weaver lab (UCSF) and the Gardel lab (University of Chicago) for sharing the T-mNG knock-in hESC line. We also thank all members of the Macara lab, especially Vaishna Vamadevan and Christian de Caestecker for valuable suggestions and advice. This work was funded by an American Heart Association postdoctoral fellowship (Award ID 23POST1018347 to L.F.), a Vanderbilt Mechanobiology fellowship (to L.F.) and a grant from the National Institutes of Health (GM070902 to I.G.M.).

Author contributions

L.F. conceived the study, performed and quantified all experiments except the QPOL, and wrote the manuscript. W.W. imaged and quantified the QPOL data. I.G.M. supervised the project, and edited the manuscript

Declaration of interest

The authors declare no competing interests.

Material & Methods

Research compliance and ethical regulation

All experiments using human ESCs were performed using the WA09 (H9) cell line under the supervision of the Vanderbilt Institutional Human Pluripotent Cell Research Oversight Committee (protocol IRB no. 160146). No cells were sourced directly from human embryos.

Reagents

Common laboratory reagents used in this study are listed in Supplementary Table 1

Cell culture and maintenance

Human GM25256 iPSCs were obtained from the Coriell Institute. The mEGFP–CTNNB1 knock-in GM25256 iPSC cell line was obtained from the Allen Cell Collection, Coriell Institute (cell ID AICS-0058-067). The human ESC line H9 (WA09) was obtained from the WiCell Research Institute. The T-mNG knock-in hESC H9 was made by Valerie Weaver lab (UCSF) and kindly

365 provided by Margaret Gardel (University of Chicago). The iPSC and ESC H9 lines were cultured
366 on Matrigel-coated six-well plates (Matrigel diluted at 42 µg ml−1 in DMEM/F12 medium) and
367 cultured in mTeSR1 medium. The medium was changed daily until the cells reached 70%
368 confluency. Cells were passaged using Gentle cell dissociation reagent for 4 min, resuspended in
369 mTseR1 medium as small clusters and replated at 1:7.
370 HEK293T cells were obtained from the ATCC. Cells were grown in 10% FBS DMEM medium and
371 passaged at 1:10 every 2-3 days.
372 All cell lines used in this study were maintained at 37 °C under 5% CO_2.
373
374 Cell freezing and thawing
375 Human iPSCs and ESCs were harvested from culture dishes using Gentle cell dissociation
376 reagent and centrifuged at 120g for 3 min. The pellets were resuspended in mTeSR1 medium
377 supplemented with 10% DMSO and aliquoted into cryovials. The cells were first transferred to
378 −80 °C for 24 h before long-term storage in liquid nitrogen. iPSCs and ESCs were slowly thawed
379 using mTeSR1, centrifuged and resuspended in mTeSR1 supplemented with 10 µM Y-27632 for
380 24 h.
381
382 Mesoderm differentiation protocol
383 Differentiation was initiated when cells reach 70-80% confluency. Cells were treated with 7.5
384 µM CHIR99021 (hereafter CHIR) diluted in RPMI media supplemented with 1X B27 minus
385 insulin and 100U/mL Penicillin and 100 µg/mL streptomycin (1X) for up to 72 hours.
386 For pharmaceutical inhibition of contractility, cells were pre-treated overnight with respective
387 drug or vehicle (water) diluted in mTeSR1. Differentiation was initiated by switching to CHIR
388 media as described above, supplemented with respective drug or vehicle (water). Similarly, cells
389 were pre-induced overnight with Doxycycline or vehicle (water) diluted in mTeSR1 before
390 initiating the differentiation protocol in the presence of Doxycycline or water. For concentration
391 of each drug, please refer to Supplementary Table 1.
392
393 Lentiviral preparation
394 HEK193T were grown at 40% confluency in 10 cm plate and transfected using Calcium-
395 Phosphate. Briefly, 20 µg of lentiviral plasmid, 15 µg of pSPAX2 (Addgene #8454) and 6 µg

396 pMD2G (Addgene #12260) were mixed with 450 µL sterile water and 50 µL of 2.5M $CaCl_2$
397 solution, previously filter sterilized. DNA mixture was added dropwise into 500 µL of 2X HeBS
398 (50 mM HEPES, 10 mM KCl, 12 mM dextrose, 280 mM NaCl and 1.5 mM Na2PO4, pH 7.04) with
399 constant vortexing. Solution was added dropwise on HEK 293T cells for 6h. Medium was
400 replaced with 8mL of fresh 10% FBS DMEM medium for 48h. Supernatant was filtered through a
401 0.22 µm membrane and concentrated using a 100kDa cut-off Amicon centrigal unit. Aliquots
402 were frozen at -80 °C.
403
404 SDS-PAGE and Western blotting
405 Cells were washed with ice cold 1X PBS and lysed with 70 µL RIPA buffer (150 mM NaCl, 10 mM
406 Tris–HCl pH 7.5, 1 mM EDTA, 1% Triton X-100, 0.1% SDS) supplemented with and 1X protease
407 and phosphatase inhibitors. Mechanical disruption was performed by scrapping the cells off the
408 plate, transferring the lysate into a 1.5mL Eppendorff tube and vortexing for 5 seconds followed
409 by 5 min incubation on ice. Soluble proteins were collected by centrifugation at 16000 g (13200
410 rpm) for 10min at 4°C. Protein concentration was measured using Precision Red following the
411 manufacturer's instructions. Lysates in sample buffer were boiled for 5min.
412 For ppMLC blotting, cells were washed with 1X PBS and directly lysed using 250 µL of boiling 1X
413 Sample buffer. Lysates were sonicated 3 times for 10 seconds with 60 seconds incubation on ice
414 between each blast.
415 30 µg of proteins were resolved on 1.5mm thick bis-tris acrylamide gels and transferred onto
416 0.2 µm nitrocellulose membrane using BioRad wet transfer system (50 V for 2hours).
417 Membranes were blocked for > 30min at room temperature (RT) with 5% BSA in 1X TBS-T
418 (10 mM Tris pH 8.0, 150 mM NaCl and 0.5% Tween 20) and incubated overnight at 4°C and
419 gentle rocking with primary antibodies diluted in blocking buffer (Supplementary Table 2).
420 Membranes were washed 3 times with 1X TBS-T and incubated for 1h at RT with AlexaFluor-
421 conjugated secondary antibodies (Supplementary Table 2). After 3 additional washes in 1X TBS-
422 T, membranes were scanned using Li-Cor Odyssey CLx system, analyzed and processed using
423 Image StudioLite v. 5.2.
424
425 Immunofluorescence

426 Cells were cultured on Matrigel-coated Ø 12mm coverglass, fixed with 4% paraformaldehyde for
427 10min, permeabilized for 5min at RT (20mM Glycine, 0.05% Triton X-100 in 1X PBS), and
428 incubated with blocking buffer for > 30min (5% BSA in 1X PBS). Coverslips were transferred into
429 a dark humidified chamber and incubated with primary and AlexaFluor-conjugated secondary
430 antibodies (Supplementary Table 2) diluted in blocking buffer for 2 hours. Coverslips were
431 washed in 1X PBS and mounted on glass slide using Fluoromount-G mounting solution.
432 For ppMLC staining, samples were incubated overnight with primary antibody.
433
434 Image acquisition, analysis and processing
435 Micrographs were obtained using an inverted Nikon A1-R confocal microscope equipped with a
436 x20 objective (Numerical aperture NA 0.75), a x40 oil objective (NA 1.20) and a x100 oil
437 objective (NA 1.40). Z-stacks covering the entire cell height were acquired. Maximum Intensity
438 Projections were obtained and images were analyzed and processed using Fiji (version
439 2.1.0/1.54f).
440
441 MYPT1^{CA}-NES-mNeonGreen cloning strategy
442 gBlock corresponding to truncated human MYPT1 (aa 1-300) was built in fusion with a PKI super
443 NES and mNeonGreen sequence. gBlock was amplified using Fusion polymerase and the
444 following primers: Fwd 5'-CTGCTGACCGGTACCATGGCGGACGCGAAGC-3' and Rev 5'-
445 CATCATACGCGTCTACGATCCGCCACCGC-3'. PCR product and recipient backbone (pInducer10b-
446 HA-KRas G12V Addgene #164928) were digested with AgeI-HF and MluI-HF for 1h at 37°C, gel
447 purified and ligated overnight at 16°C using T4 ligase. Ligation reactions were transformed into
448 chemically competent E.Coli Stbl3 strain by heatshock (45 sec at 42°C) and selected on
449 Ampicillin plate. Clones were isolated and set up for MiniPrep (QIAprep Spin MiniPrep kit). The
450 presence of the insert was confirmed by restriction digest check. Positive clones were sent for
451 full plasmid sequencing provided by Genewiz Plasmid-EZ service before MidiPrep using Takara
452 Bio NucleoBond XtraMidi kit.
453
454 Flow cytometry analysis
455 T-mNeonGreen knock-in hESC were transduced with a lentivector expressing Histone 2B-
456 mScarlet (pWPI-H2B-mScarlet). Cells were pre-treated overnight with Vehicle (water) or 10 µM

457 Y-27632. Differentiation was initiated for 24 hours as described above and cells were harvested
458 as single cells. Briefly, cells were washed and gentle cell dissociation buffer was added for 8 min
459 at 37°C. Cell suspension was centrifuged and resuspended in 500 µL PBS. Cells were passed
460 through a Ø 40 µm strainer directly into 500 µL of 8% PFA (final concentration 4%) and fixed for
461 10 min on a wheel before sending them for cytometry using a 5-laser Fortessa analyzer (70 µm
462 nozzle). Singlets were selected based of forward and side scatter. mScarlet (PE-Texas-RedA) and
463 mNeonGreen (GFP-A) population were selected by drawing a gate on double negative WT hESC
464 shifted by one order of magnitude. Percentage of mNeonGreen/mScarlet double positive was
465 reported.
466
467 RNA isolation and RT-qPCR
468 Cells were washed and RNAs were isolated using RNeasy mini kit following manufacturer's
469 instructions. 1 µg of RNA was reverse transcribed to cDNA using the SuperScript III first-strand
470 synthesis kit. cDNA was diluted 1:5 in water and mixed with Maxima SYBR Green/1mM of each
471 primer (Supplementary Table 3). Quantitative PCR was performed on a BioRad CFX96
472 thermocycler. C_t values from technical triplicates were averaged and normalized to GAPDH using
473 the $\Delta\Delta C_t$ formula.
474
475 Cell Fractionation
476 Following appropriate treatment, cells were washed with ice cold 1X PBS and collected as single
477 cell suspension using gentle cell dissociation as previously described. Cell suspension was
478 washed with cold 1X PBS and resuspended in 500 µL of cold PBS. 100 µL of the cell suspension
479 was set aside and mixed with 30 µL of 4X sample buffer. Sample was sonicated for 15 sec at 20%
480 power 3 times, boiled 5min and stored at -20 °C (Whole Cell Lysate fraction or WCL).
481 Cell fractionation was performed using Cell signaling kit (#9038) and their protocol. Briefly, the
482 remaining 400 µL of cell suspension was centrifuged at 500 x g at 4°C for 5min. Supernatant was
483 removed and pellet was resuspended in 250 µL of CIB buffer, vortexed for 5 sec and incubated
484 on ice for 5 min. Samples were centrifuged at 500 x g at 4°C for 5min and supernatant was
485 stored in pre-chilled tube (= Cytoplasmic fraction). Pellet was resuspended in 250 µL of MIB
486 buffer, vortexed for 15 sec and incubated on ice for 5 min. Samples were centrifuged at 8000 x g
487 at 4°C for 5min and supernatant was discarded (= Membrane and organelle fraction). Pellet was

488 resupended in 125 µL of CyNIB buffer, sonicated for 5 sec at 20% power 3 times (cytoskeletal
489 and nuclear fraction). Each fraction was mixed with the appropriate volume of 4X sample buffer
490 to obtain a final concentration of 1X. Samples were boiled for 5min and centrifuged before
491 loading 15 µL.
492
493 Reproducibility and statistics
494 All datasets were analyzed using GraphPad Prism10 (version 10.0.3). Individual measurements
495 (n) were averaged for each biological repeat (N). Datasets were tested for normality (Shapiro-
496 Wilk test) before applying the appropriate statistical test on the biological repeat (N), except if
497 mentioned differently in the figure legend. For dataset displayed as superplots, individual
498 measurements and biological repeats are represented by small and large dots respectively. Each
499 dataset for a biological repeat is color coded. Error bar represent S.D. Significance levels are
500 given as follows and exact P values are indicated in each figure: NS, not significant ($P \geq 0.05$);
501 *$P < 0.05$; **$P < 0.01$; ***$P < 0.001$; and ****$P < 0.0001$.
502 All experiments, including representative MIPs and western blots, were performed at least three
503 times independently as biological repeats, unless stated otherwise in the legends. No statistical
504 method was used to pre-determine the sample size, the experiments were not randomized and
505 the investigators were not blinded to allocation during experiments and outcome assessment.
506
507 **Figure legends**
508 Figure 1: Pharmaceutical inhibition of actomyosin contractility promotes hiPSc and hESC
509 conversion to the mesoderm lineage
510 A, B – Immunoblot of Brachyury during hiPSC-to-mesoderm commitment (0-48h) in the
511 presence (+ Y-27632) or absence (+ Veh) of ROCK inhibitor. Molecular weights (M.W.) are
512 displayed on the right side (A). Brachyury expression was quantified by densitometry and
513 normalized to α-Tubulin as loading control across N=3 independent biological repeats (B). Mean
514 and S.D. are displayed. Two-tailed unpaired t test was performed.
515 C-F – Relative expression of mesoderm markers (*MESP1, TBX6*) (C, D) and EMT markers (*SNAI1,*
516 *SNAI2*) (E, F) 48h post CHIR treatment in the presence (+Y-27) or absence (+Veh) of ROCK
517 inhibitor. N=3 independent biological repeats except for *MESP1* N=4 independent biological
518 repeats. Mean and S.D. are displayed. Two-tailed unpaired t test was performed.

519 G-I – Representative MaxIP immunofluorescences during hiPSC-to-mesoderm commitment (0-
520 48h) in the presence (+ Y-27632) or absence (+ Veh) of ROCK inhibitor. Cells were stained with a
521 nuclear marker (DNA), EMT marker (ZO-1 – Inverted LUT) and Mesoderm marker (T/Bra–
522 Inverted LUT). Scale bar = 50 µm (G). Quantification of Brachyury expression (H) and ZO-1
523 intactness (I) is represented as violin plots with individual measurements (small dots) averaged
524 for each biological repeat (large dots). Median (Plain red line) and quartiles (Dotted black lines).
525 n=10-15 technical repeats across N=3 independent biological repeats. One-way ANOVA with
526 Tukey's multiple comparisons post-test was performed on biological repeats.
527 J, K – Analysis of Brachyury expression by flow cytometry following 24h CHIR treatment in the
528 presence (+Y-27632) or absence (+Veh) of ROCK inhibitor using Bra-mNeonGreen knock-in H9
529 hESC line (J). Quantification of the percentage of cells mNeonGreen-positive from N=4
530 independent biological repeats. Mean and S.D. are displayed. Two-tailed unpaired t test was
531 performed (K).
532 L, M – Immunoblot of Brachyury (mesoderm) and Nanog (Pluripotency marker) using hESC H9 in
533 the presence (+ Y-27632) or absence (+ Veh) of ROCK inhibitor. Molecular weights (M.W.) are
534 displayed on the right side (L). Brachyury expression was quantified by densitometry and
535 normalized to α-Tubulin as loading control across N=3 independent biological repeats (M).
536 Mean and S.D. are displayed. Two-tailed unpaired t test was performed.
537 N, O – Representative MaxIP immunofluorescence of hiPSCs treated with a MLCK inhibitor (ML-
538 7) or Vehicle (DMSO) and stained for nuclei (DNA) and phospho T18/S19 Myosin Light Chain 2
539 (ppMLC2 – Inverted LUT). Scale bar = 50 µm. Magnified views of the yellow dotted ROI are
540 shown for ppMLC2. Scale bar = 20 µm (N). Percentage of cellular area positive for ppMLC2
541 following Vehicle or ML-7 treatment is reported as violin pots. Median (Plain red line) and
542 quartiles (Dotted black lines). n=15 technical repeats across N=3 independent biological repeats.
543 Two-tailed unpaired t test was performed on the biological repeats.
544 P, Q - Immunoblot of Brachyury (mesoderm) and PARP (Cell death marker) using hiPSCs in the
545 presence (+ ML-7) or absence (+ Veh) of MLCK inhibitor at basal state (0h) and during CHIR
546 treatment (24h, 48h). Molecular weights (M.W.) are displayed on the right side (P). Brachyury
547 expression was quantified by densitometry and normalized to α-Tubulin as loading control
548 across N=3 independent biological repeats. Mean and S.D. are displayed. Mann-Whitney test

549 was performed for the 24h timepoints and two-tailed unpaired t test was performed for the 48h
550 timepoints (Q).
551
552 Figure 2: Genetic inhibition of actomyosin contractility promotes hiPSc conversion to the
553 mesoderm lineage
554 A – Summary of the main regulators of MLC phosphorylation.
555 B – Schematic representation of full length MYPT1 (1030 aa), interacting with PP1c phosphatase
556 and protein of unknown function M20. Truncation of MYPT1 Cterm Δ301-1030 leads to a
557 constitutive recruitment and activation of PP1C. Truncated MYPT1 was fused with NES-
558 mNeonGreen and is referred to as MYPT1^{CA}-NES-mNG.
559 C – Immunoblot of phospho T18/S19 MLC2 (ppMLC2) and total MLC2 in WT hiPSCs treated with
560 Doxycycline or hiPSC expressing MYPT1^{CA}-NES-mNG in the presence or absence of Doxycycline.
561 α-Tubulin was used as loading control. Molecular weights (M.W.) are displayed on the right side
562 D, E – Representative MaxIP immunofluorescence of hiPSC expressing MYPT1^{CA}-NES-mNG and
563 treated or not with Doxycycline. Cells were fixed and stained for phospho T18/S19 MLC2
564 (ppML2 - Magenta), DNA (blue) and tight junction marker ZO-1 (Orange). Scale bar = 50 µm (D).
565 Fraction of the cellular area positive for ppMLC2 following Doxycycline induction of MYPT1^{CA}-
566 NES-mNG hiPSC and reported as violin plots. Median (Plain red line) and quartiles (Dotted black
567 lines). n=32 technical repeats across N=3 independent biological repeats. Two-tailed unpaired t
568 test was performed on the biological repeats (E).
569 F, G – Representative immunoblot for Brachyury (mesoderm marker), Snail and Slug (EMT
570 markers) using WT and MYPT1^{CA}-NES-mNG hiPSCs, following CHIR treatment (0h-48h) in the
571 presence or absence of Doxycycline. Molecular weights (M.W.) are displayed on the right side
572 (F). Brachyury expression was quantified by densitometry and normalized to α-Tubulin as
573 loading control across N=3-4 independent biological repeats. Mean and S.D. are displayed. A
574 one-way ANOVA with Tukey's multiple comparisons post-test was performed (G).
575 H – Immunoblot of PARP (cell death marker) and Brachyury (Mesoderm marker) during
576 mesoderm commitment (0h-48h CHIR) using MYPT1^{CA}-NES-mNG hiPSCs induced with
577 Doxycycline. Molecular weights (M.W.) are displayed on the right side.
578 I, J – Representative MaxIP immunofluorescences of WT and MYPT1^{CA}-NES-mNG hiPSCs treated
579 with CHIR for 24h +/- Doxycycline. Cells were stained for nuclei (DNA), EMT marker (ZO-1 –

580 Inverted LUT) and Mesoderm marker (T/Bra – Inverted LUT). Scale bar = 100 µm (I).
581 Quantification of Brachyury expression is presented as violin plots. Median (Plain red line) and
582 quartiles (Dotted black lines). n=15-16 technical repeats across N=3 independent biological
583 repeats. One-way ANOVA with Šidák's multiple comparisons post-test was performed on
584 biological repeats (J).
585
586 Figure 3: Increased actomyosin contractility is sufficient to block mesoderm commitment and
587 EMT
588 A – Experimental design for co-culture experiment. hiPSC were transduced with lentivector
589 expressing ROCK2^{CA} or MLCK^{CA}. Transduced cells are mVenus positive and are mixed with WT
590 mVenus-negative hiPSCs. ROCK2^{CA}/MLCK ^{CA} expression is induced by addition of Doxycycline 24h
591 prior to initiating mesoderm differentiation. Doxycycline induction was maintained during the 3
592 days of differentiation using CHIR before fixing and staining.
593 B-H – Representative MaxIP immunofluorescence for Brachyury (B), EOMES (D), Slug (F) and ZO-
594 1 (H) in Vehicle (H2O) and Doxycycline-induced ROCK2^{CA} co-culture. mVenus-positive cell
595 clusters are highlighted by an orange dotted line. Individual channels are inverted LUT. Scale bar
596 = 50 µm. For (H), magnified mVenus-positive and mVenus-negative areas are shown as insets.
597 Scale bar = 20 µm. Quantification of Brachyury (C), EOMES (E) and Slug-positive cells (G) is
598 reported as violin plot, comparing mVenus-positive vs mVenus-negative cluster in the presence
599 or absence of Doxycycline. For Brachyury, n = 7 (+ Veh) and n=15 (+ Dox) across N=3
600 independent biological repeats. For EOMES, n=9 across N=3 independent biological repeats. For
601 Slug, n=9 (+ Veh) and n=10 (+ Dox) across N=3 independent biological repeats. One-way ANOVA
602 with Tukey's multiple comparisons post-test was performed (C, E, G).
603
604 Figure 4: Reduced cell contractility promotes nuclear accumulation of active β-Catenin
605 A – Experiment design for treatments and cell fractionation.
606 B-C – Representative immunoblot as explained in (A). MYPT1^{CA}-NES-mNG hiPSCs were induced
607 with CHIR for 24h in the presence or absence of Doxycycline. Whole cell lysate (WCL) was
608 collected and loaded as input while cytosolic and nuclear fractions were extracted. Fraction
609 purity was probed using cytosolic (GAPDH) and nuclear (Lamin A/C) markers. Active β-Catenin
610 (non-phospho S45) enrichment was probed for each fraction and α-Tubulin was used as loading

control. Molecular weights (M.W.) are displayed on the right side (B). Quantification of active β-Catenin enrichment in the cytosolic (left) and nuclear (right) fractions. N=3 independent biological repeats. Mean and S.D. are displayed. One-way ANOVA with Šidák's multiple comparisons post-test was performed (C).

D-F – Representative confocal slice and MaxIP for active non-phospho S45 β-Catenin (Inverted LUT) and mNeonGreen respectively. MYPT1^{CA}-NES-mNG hiPSCs were fixed at 0h and 24h post CHIR treatment complemented or not with Doxycycline. Scale bar = 50 µm. Insets represent a magnified view of the active non-phospho S45 β-Catenin with an example of the nuclei binary mask overlaid (pink). Scale bar = 10 µm (D). Schematic representation of the quantification pipeline. (E). Quantification of active non-phospho S45 β-Catenin mean intensity as depicted in (E). n = 10-12 technical repeats across N=3 independent biological repeats. Mean and S.D. are displayed. One-way ANOVA with Šidák's multiple comparisons post-test was performed (F).

G – Relative expression of WNT target genes (*LEF1* and *AXIN1*) with increasing concentration of CHIR in the presence (Magenta) or absence (Cyan) of ROCK inhibitor Y-27632. N=7 independent biological repeats. Mean and S.E.M. are displayed. One-way ANOVA with Šidák's multiple comparisons post-test was performed.

<u>Supplementary Figure 1: hiPSC differentiation along the cardiac mesoderm increases actomyosin-driven contractility (Related to Figure 1)</u>

A – Bright field imaging of WT hiPSCs treated with CHIR in the presence or absence of a pan-Caspase inhibitor Q-VD-OPH. Retraction area is highlighted in yellow. Time is presented as hh:mm. Scale bar = 20 µm.

B, C – Confocal XZ orthogonal views (B) and Maximum Intensity Projections (MaxIP) (C) of hiPSCs at basal state (0h CHIR) or post-CHIR treatment (24h and 48h CHIR), stained for DNA (Cyan) and F-Actin (Grey). Scale bar = 10 µm.

D – Quantification of the monolayer height at 0h, 24h and 48h post CHIR treatment from (B). Violin plots represent individual measurements (small dots) averaged for each biological repeat (large dots). Median (Plain red line) and quartiles (Dotted black lines). n=32 technical repeats across N=7 independent biological repeats. A Kruskal-Wallis test with Dunn's multiple comparison post-test was performed on biological repeats.

641 E, F – Representative MaxIP immunofluorescence of WT hiPSC during CHIR treatment. Fixed
642 cells were stained for DNA marker (Hoechst). Scale bar = 20 µm (E). Quantification of average
643 nuclear size from n=15 fields of view across N=3 independent biological repeats. Median (Plain
644 red line) and quartiles (Dotted black lines) are displayed. Two-tailed unpaired t test was
645 performed (F).
646 G – Correlation of cell area over cell density for each field of view during CHIR treatment.
647 Biological repeats are color-coded. Pearson correlation coefficient is displayed.
648 H – Representative MaxIP immunofluorescence of hiPSCs at basal state (0h) or post-CHIR
649 treatment (24 and 48h) stained for phospho T18/S19 MLC2 (ppMLC2). Pixels are color-coded by
650 intensity using the fire LUT.
651 I – Percentage of total imaged area that is ppMLC2-positive at 0h, 24h, 48h post CHIR is
652 reported as violin plots. Median (Plain red line) and quartiles (Dotted black lines). n=15
653 technical repeats across N=3 independent biological repeats. A Kruskal-Wallis test with Dunn's
654 multiple comparison post-test was performed on the technical repeats.
655 J – Retardance measurements obtained from hiPSCs at basal state (0h), post-CHIR treatment
656 (24h, 48h, 72h) or treated with Y-27632 at 0h (Y-27) using Quantitative Polarization Microscopy
657 imaging. Median (Plain red line) and quartiles (Dotted black lines). n=240 technical repeats for
658 0h, 24h, 48h, 72h and n=120 technical repeats for Y-27 across N=3 independent biological
659 repeats. A one-way ANOVA with Šidák's multiple comparisons post-test was performed on the
660 biological repeats.
661
662 <u>Supplementary Figure 2: Pharmaceutical inhibition of actomyosin contractility promotes hiPSc</u>
663 <u>and hESC conversion to the mesoderm lineage (Related to Figure 2)</u>
664 A, B - Representative MaxIP immunofluorescences of hiPSCs treated with a ROCK inhibitor (Y-
665 27632) or Vehicle (H_2O) and stained for nuclei marker (DNA) and phospho T18/S19 Myosin Light
666 Chain 2 (ppMLC2 – Inverted LUT). Scale bar = 50 µm. Magnified views of the yellow dotted ROI
667 are shown for ppMLC2. Scale bar = 20 µm (A). Fraction of the cellular area positive for ppMLC2
668 following Y-27632 treatment and reported as violin pots. Median (Plain red line) and quartiles
669 (Dotted black lines). n=30 technical repeats across N=3 independent biological repeats. Two-
670 tailed unpaired t test was performed on the biological repeats (B).

671 C – Relative expression of unrelated genes 48h post CHIR treatment in the presence (+Y-27) or
672 absence (+Veh) of ROCK inhibitor. N=4 independent biological repeats. Mean and S.D. are
673 displayed. Two-tailed unpaired t test was performed.
674 D - Representative MaxIP immunofluorescences of hiPSC treated 48h with CHIR in the presence
675 (+ Y-27632) or absence (+ Veh) of ROCK inhibitor. Cells were stained for nuclei marker (DNA),
676 EMT markers (ZO-1 and Slug – Inverted LUT). Scale bar = 50 µm.
677 E, F - Representative MaxIP immunofluorescences of hiPSCs treated with a ROCK inhibitor (H-
678 1152) or Vehicle (H_2O) and stained for nuclei marker (DNA) and phospho T18/S19 Myosin Light
679 Chain 2 (ppMLC2 – Inverted LUT). Scale bar = 50 µm. Magnified views of the yellow dotted ROI
680 are shown for ppMLC2. Scale bar = 20 µm (E). Fraction of the cellular area positive for ppMLC2
681 following H-1152 treatment and reported as violin pots. Median (Plain red line) and quartiles
682 (Dotted black lines). n=15 technical repeats across N=3 independent biological repeats. Two-
683 tailed unpaired t test was performed on the biological repeats (F).
684 G-K - Relative expression of mesoderm markers (*TBXT*, *MESP1, TBX6*) (G-I) and EMT markers
685 (*SNAI1, SNAI2*) (J, K) 48h post CHIR treatment in the presence (+H-1152) or absence (+Veh) of
686 ROCK inhibitor. N=3 independent biological repeats. Mean and S.D. are displayed. Two-tailed
687 unpaired t test was performed.
688 L – Immunoblot probing for mesoderm marker expression (T/Bra) and cell death marker (PARP
689 cleavage) during hiPSC-to-mesoderm commitment (0h-48h CHIR) in the presence of ROCK
690 inhibitor (+H-1152). Addition of the pan-caspases inhibitor Q-VD-OPH (+ Q-VD) to the
691 differentiation medium totally blocks mesoderm commitment and was used as negative control.
692 α-Tubulin was used as loading control. Molecular weights (M.W.) are displayed on the right side.
693 M – Representative MaxIP immunofluorescences for mesoderm marker Brachyury (T/Bra –
694 Inverted LUT) and nuclei. Cells were fixed 24h post-CHIR treatment in the presence or absence
695 of ROCK inhibitor H-1152.
696 N-P – Representative immunoblot of PARP (cell death), T/Bra (mesoderm), Oct4 and Nanog
697 (Pluripotency markers) using hESC H9 in the presence (+ Y-27632) or absence (+ Veh) of ROCK
698 inhibitor. Molecular weights (M.W.) are displayed on the right side (N). PARP cleavage (O) and
699 Nanog expression (P) was quantified by densitometry and normalized to α-Tubulin as loading
700 control across N=4 (PARP) and N=3 (Nanog) independent biological repeats. Mean and S.D. are
701 displayed. Two-tailed unpaired t test was performed.

702

703 Supplementary Figure 3: Increased actomyosin contractility is sufficient to block mesoderm
704 commitment and EMT (Related to Figure 3)

705 A – Representative MaxIP immunofluorescence of Doxycycline-induced ROCK2^{CA} hiPSCs
706 (mVenus-positive) mixed with WT hiPSCs (mVenus-negative). Cells were stained for DNA
707 (Nuclei), F-actin (top – Inverted LUT) and phospho T18/S19 Myosin Light Chain 2 (Bottom -
708 ppMLC2 – Inverted LUT). Scale bar = 50 µm. Magnified views comparing mVenus-positive
709 (Green dotted ROI) and mVenus-negative (Black dotted ROI) areas are shown for F-Actin and
710 ppMLC2. Scale bar = 10 µm.

711 B – Percentage of the ROI area positive for mVenus based on cluster considered as mVenus-
712 Negative and Positive using the ROCK2^{CA} line. On average, mVenus negative clusters have <15%
713 of their area positive for mVenus. Mean and S.E.M are displayed. n=7 (no Dox) and n=15 fields
714 of view (+Dox) across N=3 independent biological experiments.

715 C – Representative MaxIP immunofluorescence of Doxycycline-induced MLCK^{CA} hiPSCs (mVenus-
716 positive) mixed with WT hiPSCs (mVenus-negative). Cells were stained for DNA (Nuclei), F-actin
717 (top – Inverted LUT) and phospho T18/S19 Myosin Light Chain 2 (Bottom - ppMLC2 – Inverted
718 LUT). Scale bar = 50 µm. Magnified views comparing mVenus-positive (Green dotted ROI) and
719 mVenus-negative (Black dotted ROI) areas are shown for F-Actin and ppMLC2. Scale bar = 10
720 µm.

721 D – Percentage of the ROI area positive for mVenus based on cluster considered as mVenus-
722 Negative and Positive using the MLCK^{CA} line. On average, mVenus negative clusters have <15%
723 of their area positive for mVenus. Mean and S.E.M are displayed. n=7 (no Dox) and n=18 fields
724 of view (+Dox) across N=3 independent biological experiments.

725 E, F - Representative MaxIP immunofluorescence for Brachyury in Vehicle (+Veh) and
726 Doxycycline-induced MLCK^{CA} co-culture. mVenus-positive cell clusters are highlighted by an
727 orange dotted line. Individual channels are inverted LUT. Scale bar = 50 µm (E). Percentage of
728 Brachyury-positive nuclei is reported as violin plot, comparing mVenus-positive vs mVenus-
729 negative cluster in the presence or absence of Doxycycline. Median (Plain red line) and quartiles
730 (Dotted black lines). n=7 (+Veh) and n=18 (+ Dox) fields of view (small dots) across N=3
731 independent biological repeats (large dots). One-way ANOVA with Tukey's multiple comparisons
732 post-test was performed (F).

733 G - Representative MaxIP immunofluorescence for EOMES, Slug and ZO-1 in Doxycycline-
734 induced MLCK^{CA} co-culture. mVenus-positive cell clusters are highlighted by an orange dotted
735 line. Individual channels are inverted LUT. Scale bar = 50 µm.
736
737 Supplementary Figure 4: Reduced cell contractility promotes nuclear accumulation of active β-
738 Catenin (Related to Fig. 4)
739 A, B – Immunoblot for phospho S127 YAP (pYAP)and total YAP following differentiation (0-48h
740 CHIR) in the presence or absence of ROCK inhibitor Y-27632. Brachyury expression was also
741 probed as an internal positive control and α-Tubulin was used as loading control. Molecular
742 weights (M.W.) are displayed on the right side (A). Ratio of phospho/total YAP was quantified
743 across N=4 independent biological repeats. Mean and S.D. are displayed. One-way ANOVA with
744 Šidák's multiple comparisons post-test was performed.
745 C – Relative expression of YAP-target genes *CTGF* and *CYR61* during differentiation in the
746 presence or absence of ROCK inhibitor Y-27632. N=4 independent biological repeats. Mean and
747 S.D. are displayed. One-way ANOVA with Šidák's multiple comparisons post-test was performed.
748 D - Relative expression of canonical WNT (*WNT3A, WNT8A*), non-canonical WNT (*WNT4*) and
749 mesoderm marker (*TBX6*) in MYPT1^{CA}-NES-mNG cells treated with CHIR (0-48h) in the presence
750 of Vehicle or Doxycycline. N=3 independent biological repeats. Mean and S.D. are displayed.
751 One-way ANOVA with Šidák's multiple comparisons post-test was performed.
752 E – Relative expression of *TBX6* and *MESP1* (mesoderm markers) following CHIR treatment in
753 the presence of Y-27632 complemented or not with 7.5 µM Porcupine inhibitor (IWP-2 or DMSO
754 respectively). N=3 independent biological repeats. Mean and S.D. are displayed. One-way
755 ANOVA with Tukey's multiple comparisons post-test was performed.
756 F – Compartment purity following fractionation was assessed by quantifying Lamin A/C and
757 GAPDH enrichment in both, cytosolic and nuclear fractions across N=4 independent biological
758 repeats.
759 G, H – Still pictures from confocal timelapse imaging of mEGFP-β-Catenin knock-in hiPSCs
760 treated with CHIR +/- Y-26732. Time is shown in hours. Scale bar = 10 µm (G). mEGFP-β-Catenin
761 intensity is reported as a scan line plot across a cell at 0h and 20h (H).
762
763 **References**

1. Firmin, J. *et al.* Mechanics of human embryo compaction. *Nature* 629, 646–651 (2024).
2. Deglincerti, A. *et al.* Self-organization of human embryonic stem cells on micropatterns. *Nat Protoc* 11, 2223–2232 (2016).
3. Muncie, J. M. *et al.* Mechanical Tension Promotes Formation of Gastrulation-like Nodes and Patterns Mesoderm Specification in Human Embryonic Stem Cells. *Dev Cell* 55, 679-694.e11 (2020).
4. Hookway, C. *et al.* A human induced pluripotent stem (hiPS) cell model for the holistic study of epithelial to mesenchymal transitions (EMTs). *BioRxiv* (2024).
5. Fort, L., Gama, V. & Macara, I. G. Stem cell conversion to the cardiac lineage requires nucleotide signalling from apoptosing cells. *Nat Cell Biol* 24, 434–447 (2022).
6. Lomakin, A. J. *et al.* The nucleus acts as a ruler tailoring cell responses to spatial constraints. *Science (1979)* 370, (2020).
7. de Leeuw, N. F., Budhathoki, R., Russell, L. J., Loerke, D. & Blankenship, J. T. Nuclei as mechanical bumpers during epithelial remodeling. *Journal of Cell Biology* 223, (2024).
8. Totsukawa, G. *et al.* Distinct roles of ROCK (Rho-kinase) and MLCK in spatial regulation of MLC phosphorylation for assembly of stress fibers and focal adhesions in 3T3 fibroblasts. *J Cell Biol* 150, 797–806 (2000).
9. Shi, Y., Ohler, L. S., de Jesus, B. N. & Dickinson, D. J. Opposing actomyosin pools generate cortical flows that establish epithelial polarity. *Biorxiv* (2024).
10. Makishima, M. *et al.* Induction of differentiation of human leukemia cells by inhibitors of myosin light chain kinase. *FEBS Lett* 287, 175–177 (1991).
11. Matsumura, F., Yamakita, Y. & Yamashiro, S. Myosin Phosphatase-targeting Subunit 1 Controls Chromatid Segregation. *Journal of Biological Chemistry* 286, 10825–10833 (2011).
12. Kiss, A., Erdődi, F. & Lontay, B. Myosin phosphatase: Unexpected functions of a long-known enzyme. *Biochimica et Biophysica Acta (BBA) - Molecular Cell Research* 1866, 2–15 (2019).
13. Yamamoto, K. *et al.* Optogenetic relaxation of actomyosin contractility uncovers mechanistic roles of cortical tension during cytokinesis. *Nat Commun* 12, 7145 (2021).
14. Stronati, E. *et al.* YAP1 regulates the self-organized fate patterning of hESC-derived gastruloids. *Stem Cell Reports* 17, 211–220 (2022).
15. Röper, J.-C. *et al.* The major β-catenin/E-cadherin junctional binding site is a primary molecular mechano-transductor of differentiation in vivo. *Elife* 7, (2018).
16. van der Wal, T. & van Amerongen, R. Walking the tight wire between cell adhesion and WNT signalling: a balancing act for β-catenin. *Open Biol* 10, (2020).
17. Orsulic, S., Huber, O., Aberle, H., Arnold, S. & Kemler, R. E-cadherin binding prevents β-catenin nuclear localization and β-catenin/LEF-1-mediated transactivation. *J Cell Sci* 112, 1237–1245 (1999).
18. Roura, S., Miravet, S., Piedra, J., de Herreros, A. G. & Duñach, M. Regulation of E-cadherin/Catenin Association by Tyrosine Phosphorylation. *Journal of Biological Chemistry* 274, 36734–36740 (1999).

19. Gayrard, C., Bernaudin, C., Déjardin, T., Seiler, C. & Borghi, N. Src- and confinement-dependent FAK activation causes E-cadherin relaxation and β-catenin activity. *Journal of Cell Biology* 217, 1063–1077 (2018).
20. Leptin, M. & Grunewald, B. Cell shape changes during gastrulation in *Drosophila*. *Development* 110, 73–84 (1990).
21. Skory, R. M. *et al.* The nuclear lamina couples mechanical forces to cell fate in the preimplantation embryo via actin organization. *Nat Commun* 14, 3101 (2023).
22. Caldarelli, P. *et al.* Self-organized tissue mechanics underlie embryonic regulation. *Nature* 633, 887–894 (2024).
23. Rozbicki, E. *et al.* Myosin-II-mediated cell shape changes and cell intercalation contribute to primitive streak formation. *Nat Cell Biol* 17, 397–408 (2015).
24. Rozbicki, E. *et al.* Myosin-II-mediated cell shape changes and cell intercalation contribute to primitive streak formation. *Nat Cell Biol* 17, 397–408 (2015).
25. Dahl, K. N., Kahn, S. M., Wilson, K. L. & Discher, D. E. The nuclear envelope lamina network has elasticity and a compressibility limit suggestive of a molecular shock absorber. *J Cell Sci* 117, 4779–4786 (2004).
26. Maître, J.-L. *et al.* Adhesion Functions in Cell Sorting by Mechanically Coupling the Cortices of Adhering Cells. *Science (1979)* 338, 253–256 (2012).
27. Krieg, M. *et al.* Tensile forces govern germ-layer organization in zebrafish. *Nat Cell Biol* 10, 429–436 (2008).
28. Turlier, H. & Maître, J.-L. Mechanics of tissue compaction. *Semin Cell Dev Biol* 47–48, 110–117 (2015).
29. Loza, A. J. *et al.* Cell density and actomyosin contractility control the organization of migrating collectives within an epithelium. *Mol Biol Cell* 27, 3459–3470 (2016).
30. Maldonado, M., Luu, R. J., Ramos, M. E. P. & Nam, J. ROCK inhibitor primes human induced pluripotent stem cells to selectively differentiate towards mesendodermal lineage via epithelial-mesenchymal transition-like modulation. *Stem Cell Res* 17, 222–227 (2016).
31. Kashkooli, L., Rozema, D., Espejo-Ramirez, L., Lasko, P. & Fagotto, F. Ectoderm to mesoderm transition by down-regulation of actomyosin contractility. *PLoS Biol* 19, e3001060 (2021).
32. Lian, X. *et al.* Robust cardiomyocyte differentiation from human pluripotent stem cells via temporal modulation of canonical Wnt signaling. *Proceedings of the National Academy of Sciences* 109, (2012).
33. Lian, X. *et al.* Directed cardiomyocyte differentiation from human pluripotent stem cells by modulating Wnt/β-catenin signaling under fully defined conditions. *Nat Protoc* 8, 162–175 (2013).
34. Brunet, T. *et al.* Evolutionary conservation of early mesoderm specification by mechanotransduction in Bilateria. *Nat Commun* 4, 2821 (2013).
35. Llewellyn, J., Charrier, A., Cuciniello, R., Helfer, E. & Dono, R. Substrate stiffness alters layer architecture and biophysics of human induced pluripotent stem cells to modulate their differentiation potential. *iScience* 27, 110557 (2024).
36. Vasic, I. *et al.* Loss of TJP1 disrupts gastrulation patterning and increases differentiation toward the germ cell lineage in human pluripotent stem cells. *Dev Cell* 58, 1477-1488.e5 (2023).
37. Pagella, P. *et al.* The time-resolved genomic impact of Wnt/β-catenin signaling. *Cell Syst* 14, 563-581.e7 (2023).

38. Yang, S. *et al.* ETV4 is a mechanical transducer linking cell crowding dynamics to lineage specification. *Nat Cell Biol* 26, 903–916 (2024).
39. Rufo, J. *et al.* An explainable map of human gastruloid morphospace reveals gastrulation failure modes and predicts teratogens. *BioRvix* (2024).
40. Dupont, S. *et al.* Role of YAP/TAZ in mechanotransduction. *Nature* 474, 179–183 (2011).
41. Pagliari, S. *et al.* YAP–TEAD1 control of cytoskeleton dynamics and intracellular tension guides human pluripotent stem cell mesoderm specification. *Cell Death Differ* 28, 1193–1207 (2021).
42. Yamaguchi, T. P., Takada, S., Yoshikawa, Y., Wu, N. & McMahon, A. P. T (Brachyury) is a direct target of Wnt3a during paraxial mesoderm specification. *Genes Dev* 13, 3185–3190 (1999).
43. Arnold, S. J. *et al.* Brachyury is a target gene of the Wnt/β-catenin signaling pathway. *Mech Dev* 91, 249–258 (2000).

Figure 1

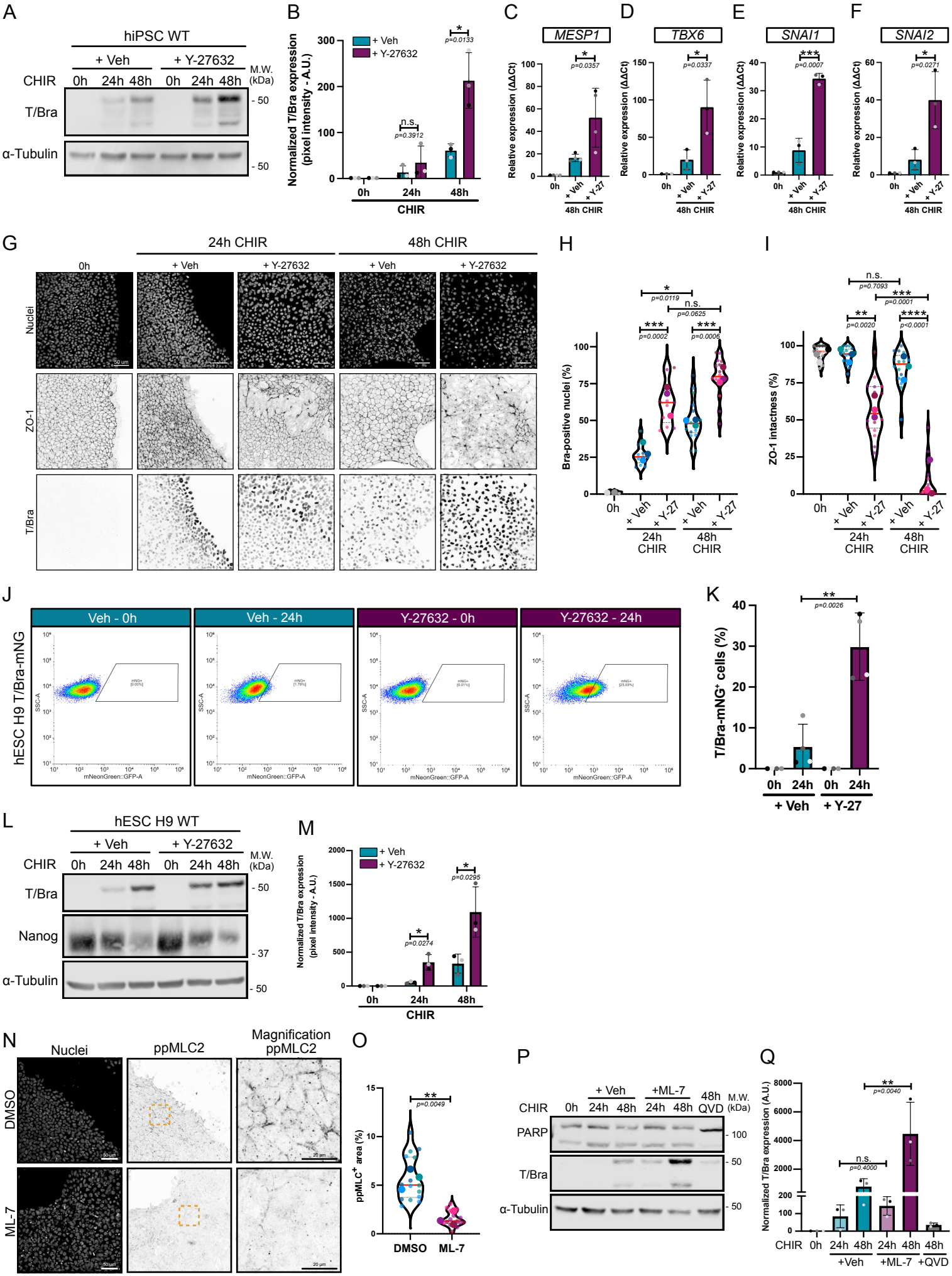
A
hiPSC WT
+ Veh
+ Y-27632
CHIR
0h 24h 48h 0h 24h 48h
M.W. (kDa)
T/Bra
α-Tubulin
- 50
- 50
B
Normalized T/Bra expression (pixel intensity - A.U.)
+ Veh
+ Y-27632
n.s. p=0.3912
* p=0.0133
0h 24h 48h
CHIR
C
MESP1
* p=0.0357
D
TBX6
* p=0.0337
E
SNAI1
*** p=0.0007
F
SNAI2
* p=0.0271
Relative expression (ΔΔCt)
0h
+ Veh
+ Y-27
48h CHIR
G
24h CHIR
48h CHIR
0h
+ Veh
+ Y-27632
Nuclei
ZO-1
T/Bra
H
Bra-positive nuclei (%)
* p=0.0119
n.s. p=0.0625
*** p=0.0002
*** p=0.0006
24h CHIR
48h CHIR
I
ZO-1 intactness (%)
n.s. p=0.7093
** p=0.0020
*** p=0.0001
**** p<0.0001
J
hESC H9 T/Bra-mNG
Veh - 0h
Veh - 24h
Y-27632 - 0h
Y-27632 - 24h
mNeonGreen::GFP-A
SSC-A
K
T/Bra-mNG+ cells (%)
** p=0.0026
0h 24h 0h 24h
+ Veh + Y-27
L
hESC H9 WT
+ Veh
+ Y-27632
CHIR
0h 24h 48h 0h 24h 48h
M.W. (kDa)
T/Bra
Nanog
α-Tubulin
- 50
- 37
- 50
M
Normalized T/Bra expression (pixel intensity - A.U.)
+ Veh
+ Y-27632
* p=0.0274
* p=0.0295
0h 24h 48h
CHIR
N
Nuclei
ppMLC2
Magnification ppMLC2
DMSO
ML-7
O
ppMLC+ area (%)
** p=0.0049
DMSO ML-7
P
CHIR
0h 24h 48h 24h 48h 48h QVD
+ Veh
+ ML-7
M.W. (kDa)
PARP
T/Bra
α-Tubulin
- 100
- 50
- 50
Q
Normalized T/Bra expression (A.U.)
** p=0.0040
n.s. p=0.4000
CHIR 0h 24h 48h 24h 48h 48h
+Veh +ML-7 +QVD

Figure 2

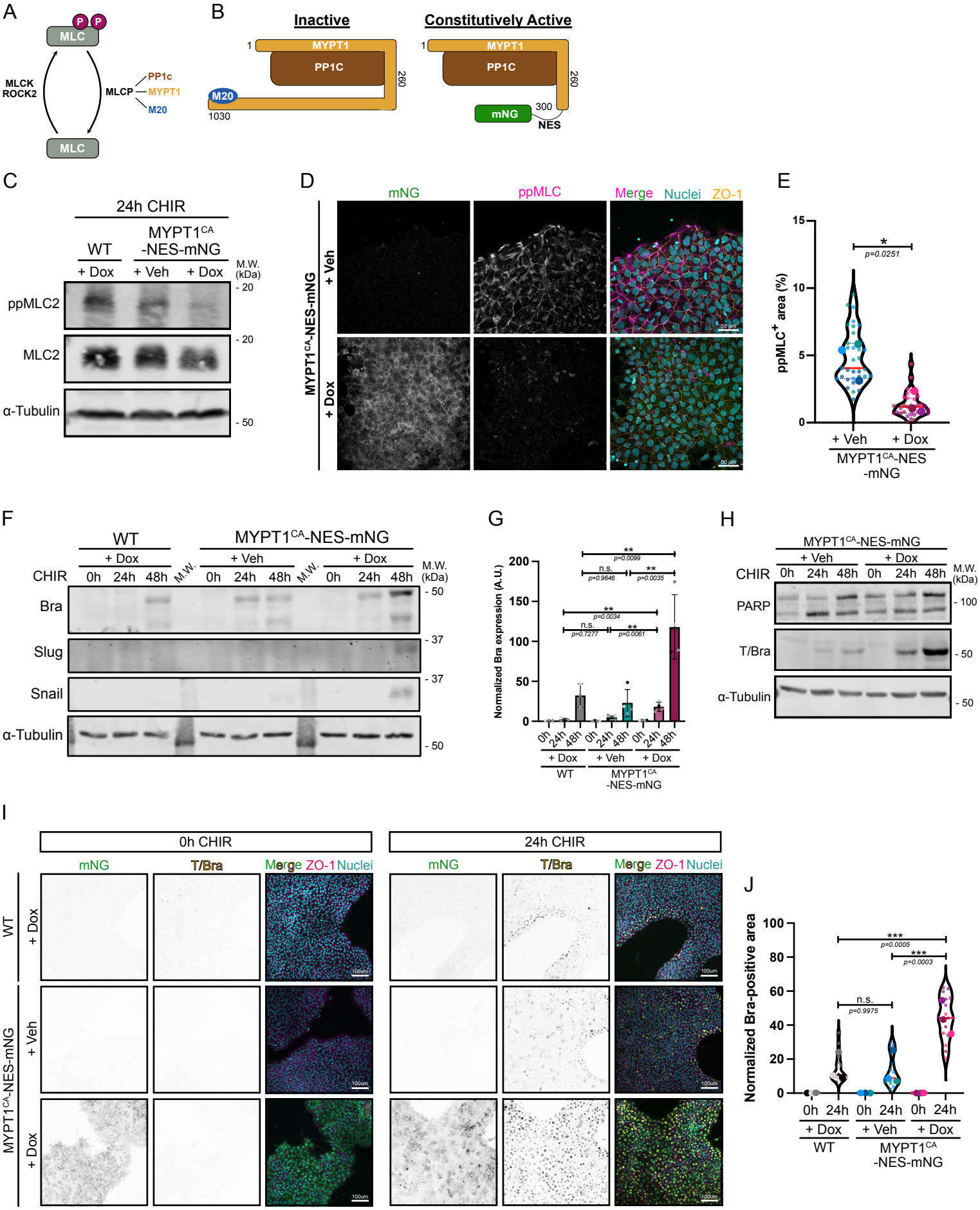
A
P P
MLC
MLCK
ROCK2
MLCP
PP1c
MYPT1
M20
MLC
B
Inactive
Constitutively Active
1
MYPT1
PP1C
260
M20
1030
1
MYPT1
PP1C
260
mNG
300
NES
C
24h CHIR
WT
MYPT1CA -NES-mNG
+ Dox
+ Veh
+ Dox
M.W. (kDa)
ppMLC2
MLC2
α-Tubulin
- 20
- 20
- 50
D
mNG
ppMLC
Merge
Nuclei
ZO-1
MYPT1CA-NES-mNG
+ Veh
+ Dox
50 µm
E
ppMLC+ area (%)
15
10
5
0
*
p=0.0251
+ Veh
+ Dox
MYPT1CA-NES -mNG
F
WT
MYPT1CA-NES-mNG
+ Dox
+ Veh
+ Dox
CHIR
0h
24h
48h
M.W.
M.W. (kDa)
Bra
Slug
Snail
α-Tubulin
- 50
- 37
- 37
- 50
G
Normalized Bra expression (A.U.)
200
150
100
50
0
**
p=0.0099
n.s.
p=0.9646
**
p=0.0035
**
p=0.0034
n.s.
p=0.7277
**
p=0.0061
0h
24h
48h
+ Dox
+ Veh
+ Dox
WT
MYPT1CA -NES-mNG
H
MYPT1CA-NES-mNG
+ Veh
+ Dox
CHIR
0h
24h
48h
M.W. (kDa)
PARP
T/Bra
α-Tubulin
- 100
- 50
- 50
I
0h CHIR
24h CHIR
mNG
T/Bra
Merge ZO-1 Nuclei
WT
+ Dox
MYPT1CA-NES-mNG
+ Veh
+ Dox
100um
J
Normalized Bra-positive area
100
80
60
40
20
0
***
p=0.0005
***
p=0.0003
n.s.
p=0.9975
0h
24h
+ Dox
+ Veh
+ Dox
WT
MYPT1CA -NES-mNG

Figure 3

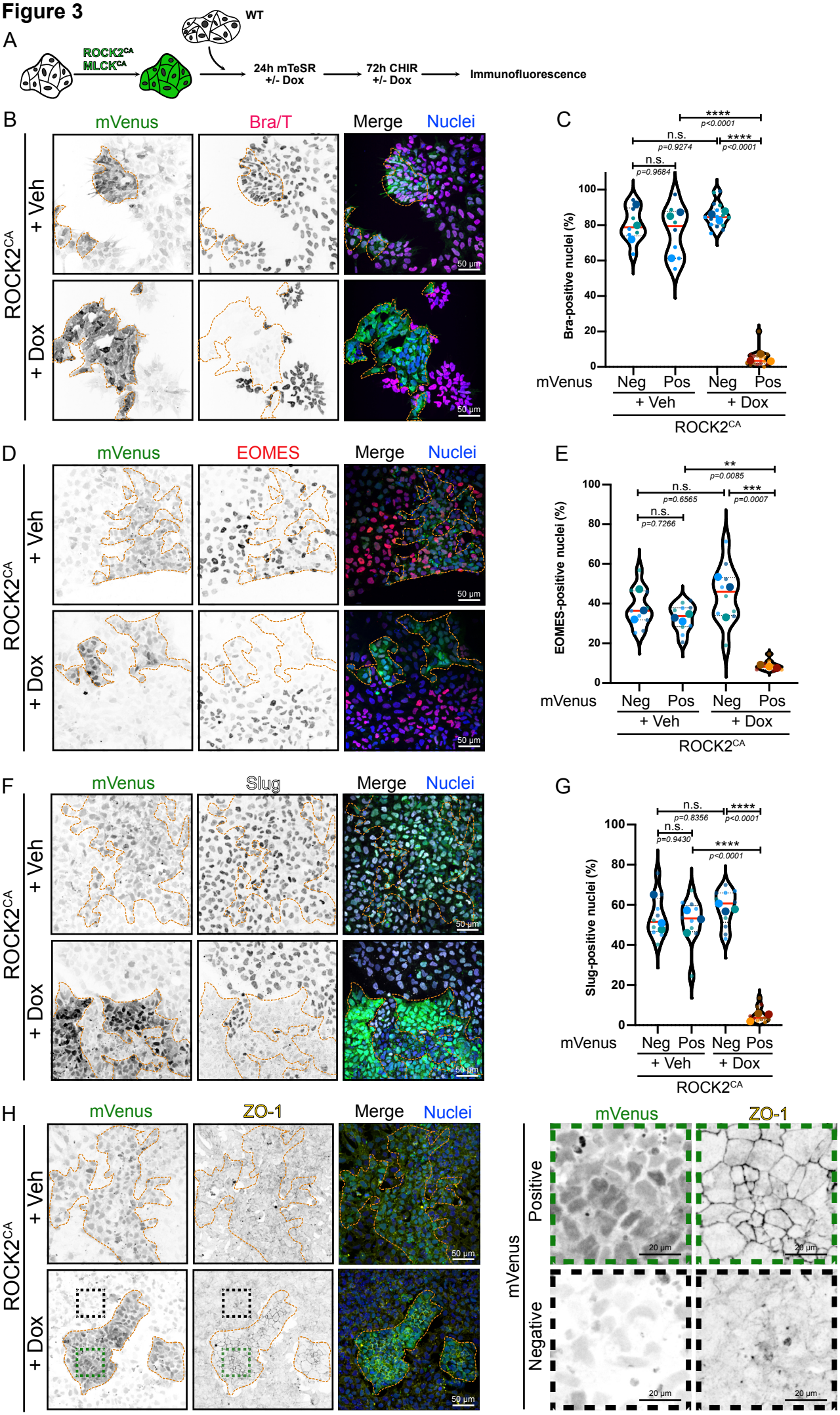
A
ROCK2CA
MLCKCA
WT
24h mTeSR
+/- Dox
72h CHIR
+/- Dox
Immunofluorescence
B
mVenus
Bra/T
Merge
Nuclei
ROCK2CA
+ Veh
+ Dox
50 µm
C
Bra-positive nuclei (%)
n.s.
p=0.9684
n.s.
p=0.9274
****
p<0.0001
****
p<0.0001
mVenus
Neg
Pos
Neg
Pos
+ Veh
+ Dox
ROCK2CA
D
mVenus
EOMES
Merge
Nuclei
ROCK2CA
+ Veh
+ Dox
50 µm
E
EOMES-positive nuclei (%)
n.s.
p=0.7266
n.s.
p=0.6565
**
p=0.0085
***
p=0.0007
mVenus
Neg
Pos
Neg
Pos
+ Veh
+ Dox
ROCK2CA
F
mVenus
Slug
Merge
Nuclei
ROCK2CA
+ Veh
+ Dox
50 µm
G
Slug-positive nuclei (%)
n.s.
p=0.9430
n.s.
p=0.8356
****
p<0.0001
****
p<0.0001
mVenus
Neg
Pos
Neg
Pos
+ Veh
+ Dox
ROCK2CA
H
mVenus
ZO-1
Merge
Nuclei
ROCK2CA
+ Veh
+ Dox
50 µm
mVenus
ZO-1
mVenus
Positive
Negative
20 µm

Figure 4

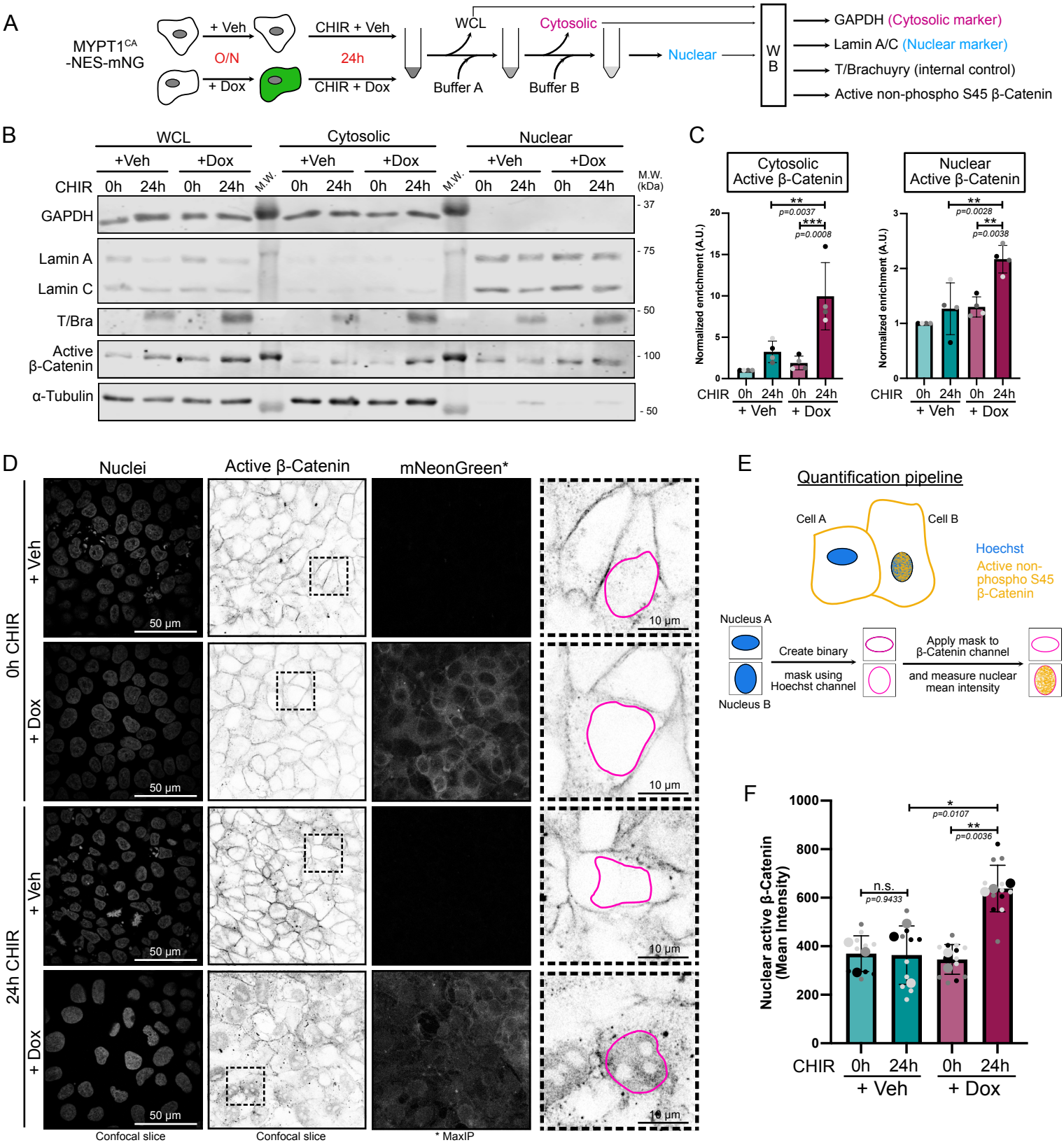
A
MYPT1CA -NES-mNG
+ Veh
O/N
+ Dox
CHIR + Veh
24h
CHIR + Dox
WCL
Buffer A
Cytosolic
Buffer B
Nuclear
WB
GAPDH (Cytosolic marker)
Lamin A/C (Nuclear marker)
T/Brachuyry (internal control)
Active non-phospho S45 β-Catenin
B
WCL
Cytosolic
Nuclear
+Veh
+Dox
CHIR 0h 24h 0h 24h
M.W.
M.W. (kDa)
GAPDH
Lamin A
Lamin C
T/Bra
Active β-Catenin
α-Tubulin
37
75
50
100
50
C
Cytosolic Active β-Catenin
Nuclear Active β-Catenin
Normalized enrichment (A.U.)
p=0.0037
p=0.0008
p=0.0028
p=0.0038
CHIR 0h 24h 0h 24h
+ Veh + Dox
D
Nuclei
Active β-Catenin
mNeonGreen*
0h CHIR
24h CHIR
+ Veh
+ Dox
50 µm
10 µm
Confocal slice
Confocal slice
* MaxIP
E
Quantification pipeline
Cell A
Cell B
Hoechst
Active non-phospho S45 β-Catenin
Nucleus A
Nucleus B
Create binary mask using Hoechst channel
Apply mask to β-Catenin channel and measure nuclear mean intensity
F
Nuclear active β-Catenin (Mean Intensity)
n.s.
p=0.9433
p=0.0107
p=0.0036
CHIR 0h 24h 0h 24h
+ Veh + Dox
G
LEF1
AXIN2
Normalized mRNA expression (ΔΔCt)
p<0.0001
p=0.0002
p=0.0234
p=0.0006
n.s.
p=0.4906
p=0.0331
p=0.0496
Veh Y-27 Veh Y-27 Veh Y-27
0h 7.5 µM 15 µM
24h CHIR

Supplementary Figure 1

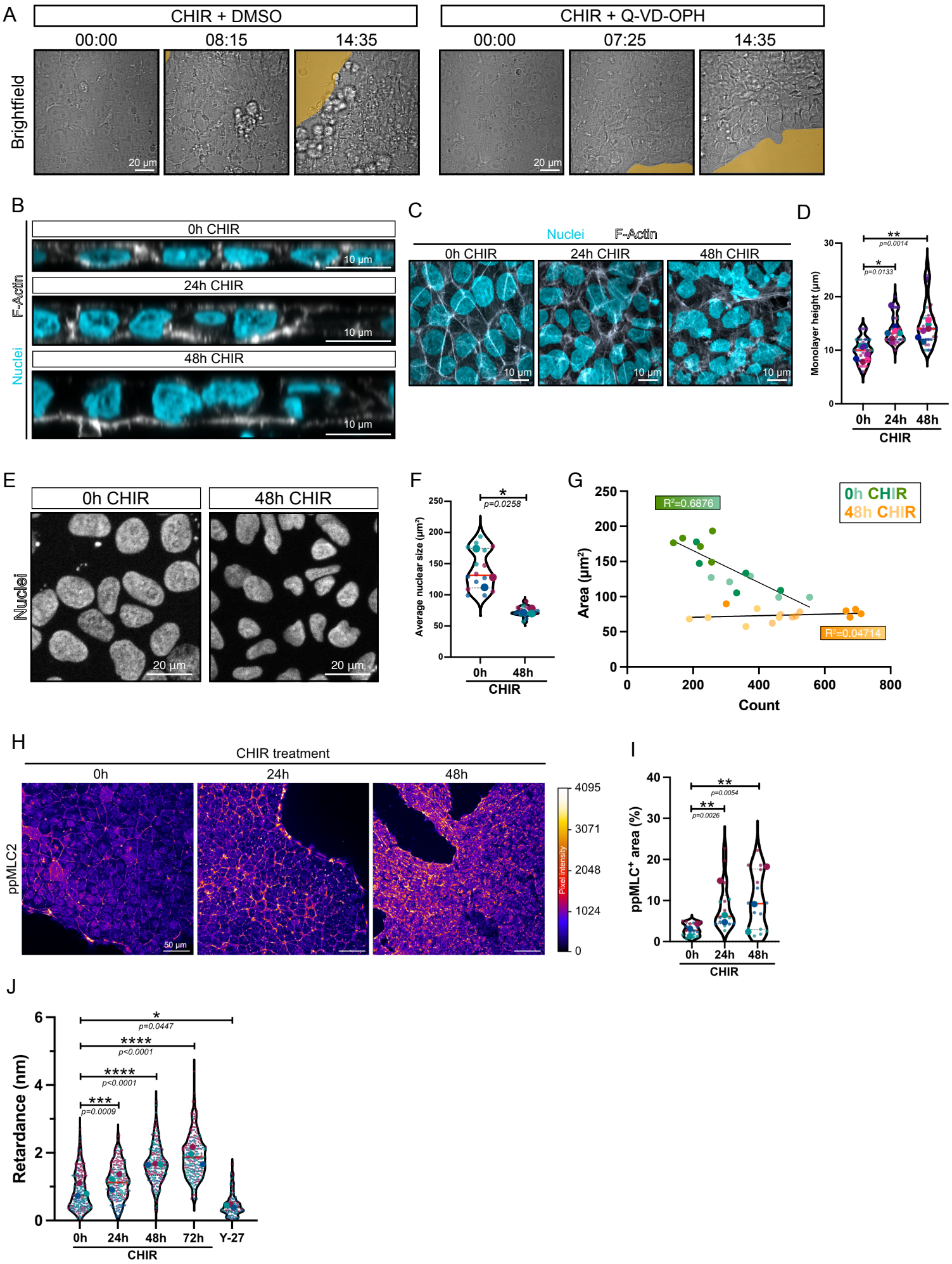

Supplementary Figure 1 (Related to Figure 2)

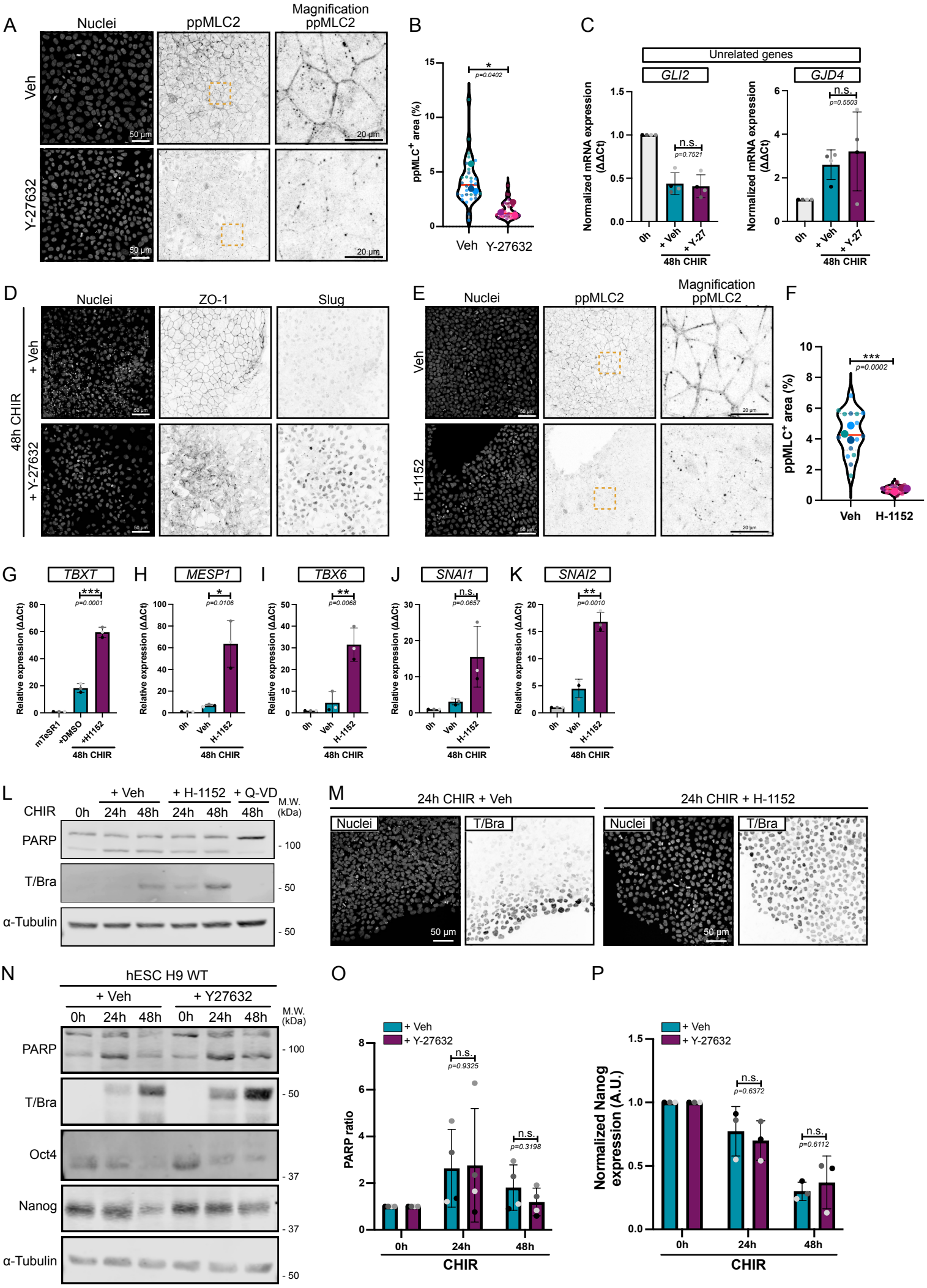

Supplementary Figure 3 (Related to Figure 3)

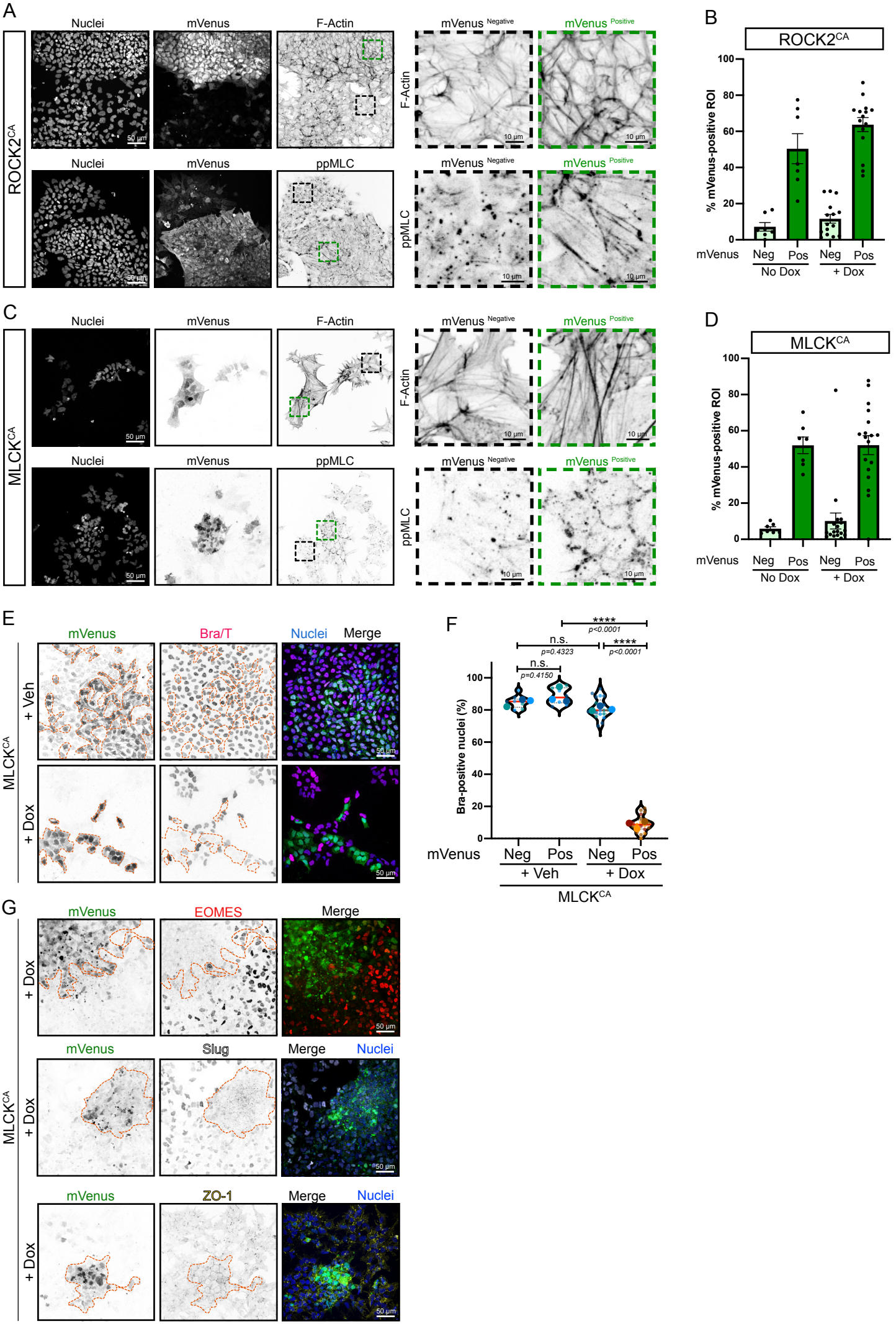
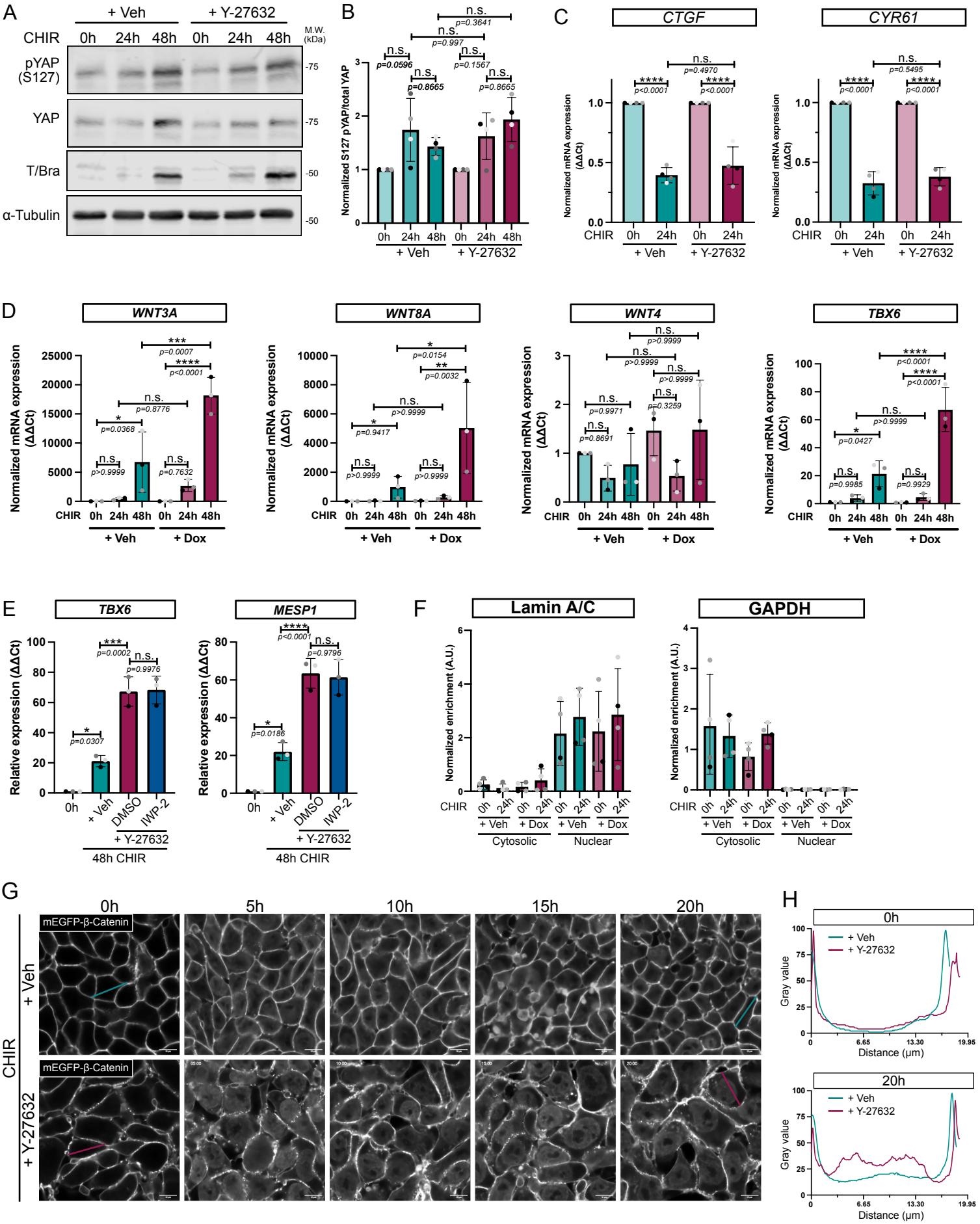
Supplementary Figure 4 (Related to Figure 4)